Available online at www.sciencedirect.com
SCIENCE DIRECT®
Earth and Planetary Science Letters 244 (2006) 133–154
EPSL
www.elsevier.com/locate/epsl

Inferring upper-mantle temperatures from seismic and geochemical constraints: Implications for Kaapvaal craton

O.L. Kuskov [a,b,*], V.A. Kronrod [b], H. Annersten [a]

[a] *Department of Earth Sciences, Uppsala University, Villavagen 16, S-752 36 Uppsala, Sweden*
[b] *V.I.Vernadsky Institute of Geochemistry and Analytical Chemistry, Russian Academy of Sciences, Kosygin Str. 19, 119991 Moscow B-334, Russian Federation*

Received 10 June 2005; received in revised form 9 February 2006; accepted 9 February 2006
Available online 13 March 2006
Editor: S. King

Abstract

Based on self-consistent thermodynamic approach, we infer the temperature distribution models at 100 to 300 km depth for the upper mantle beneath the Kaapvaal craton from absolute P- and S-wave velocities and geochemical constraints (garnet-bearing lherzolite xenoliths, average composition of garnet peridotite and primitive mantle composition). For the computation of phase equilibrium relations, we have used a method of minimization of the total Gibbs free energy combined with a Mie-Grüneisen equation of state. Our forward calculation of phase equilibria, seismic velocities and density and inverse calculation of temperature include anharmonic and anelastic parameters as well as mineral reaction effects, including phase proportions and chemical compositions of coexisting phases. Sensitivity of density and velocities to temperature, pressure and composition was studied. Calculated velocities are between the fastest and slowest seismic models reported for southern Africa. The estimated temperatures depend rather strongly on bulk composition and proportion of phases stable at various depths of the upper mantle. The relatively small differences between the xenolith compositions translate into substantial variations in inferred temperature. Temperatures inferred from the IASP91 model and from some of regional models beneath the Kaapvaal craton, irrespective of the composition model, display an inflection with a negative temperature gradient at depths below ~200–220 km, leading to unrealistic temperature behavior. We find that the cratonic upper mantle cannot be treated as uniform in terms of bulk composition because a fixed composition leads to a non-physical behavior of geotherms. A sharp change in composition from depleted garnet peridotite to fertile pyrolitic material seems unable to explain inflexions of geotherms as well as an anticorrelated behavior for T_P and T_S. To avoid temperature inflexions, a continuous change in composition and a substantial increase in fertility (gradual increase in FeO, Al_2O_3 and CaO content) at depths between 200 and 275 km are required to get monotonous temperature profiles. The mantle beneath the Kaapvaal craton is chemically stratified: an upper layer at depths between 100 and ~175 km consisting of depleted garnet peridotite and a lower layer (200–275 km) made of a more fertile material. At depths of about 275 km, Kaapvaal cratonic mantle does not differ from normal mantle. S-velocity and density model for southern Africa is constructed. The results indicate the possibility of the existence of a solid-state low-velocity zone, which may be associated with temperature gradients alone without hydrous phases and partial melting.

Keywords: temperature; composition; Kaapvaal craton; upper mantle

* Corresponding author. V.I.Vernadsky Institute of Geochemistry and Analytical Chemistry, Russian Academy of Sciences, Kosygin Str. 19, 119991 Moscow B-334, Russian Federation. Tel.: +7 495 1378614; fax: +7 495 9382054.
E-mail addresses: kuskov@geokhi.ru, ol_kuskov@mail.ru (O.L. Kuskov), va_kronrod@mail.ru (V.A. Kronrod), Hans.Annersten@geo.uu.se (H. Annersten).

0012-821X/$ - see front matter © 2006 Elsevier B.V. All rights reserved.
doi:10.1016/j.epsl.2006.02.016

1. Introduction

Quantitative estimation of the temperature distribution in the Earth's mantle is a key problem in petrology and geophysics. Geophysical and geochemical data alone are insufficient to constrain mantle temperatures. Seismic and thermal studies show both seismic heterogeneity and substantial variations in the distribution of temperature in the continental upper mantle [1,2]. Thermal models are uncertain because of the large uncertainties in the values of crustal heat production [3–5]. Despite the uncertainties in geotherms predicted from seismic models, seismic velocities may provide an alternative source of information of thermal regime of the upper mantle [6–8]. There have been numerous studies that have explored the relationship between seismic velocities, composition and temperature [9–13].

Recently, an attempt was performed to estimate temperature variations in the upper mantle of Europe, North America, Australia and East Antarctica from P- and S-wave velocity models [14–19], assuming that compositional variations are known. It was shown that geophysical and petrological observations can be explained mainly by variations of mantle temperatures whereas small variations in chemical and phase compositions have no significant influence on seismic properties. However, a study of velocity–temperature–attenuation correlations indicates that a significant part of the velocity anomalies in the continental upper mantle could be associated with compositional heterogeneity [20]. Composition, however, still remains the most important factor for the density of the continental roots [21–24], for understanding the nature of the mantle discontinuities [25–28] and for the dynamical behavior of the mantle [29].

Several key aspects of the seismic and thermal structure and chemical composition of the continental mantle are uncertain and merit further investigation. The internal structure of the mantle depends strongly on its composition and thermal regime. Available seismic models do not give direct compositional information, whereas geochemical studies of peridotite xenoliths provide unique information about the compositional heterogeneity and evolution of the upper mantle, but do not give direct information about its seismic structure. Because the effects of temperature and composition on seismic velocities are difficult to separate, geophysical observations should be interpreted in conjunction with geochemical studies. Using self-consistent thermodynamic parameters for minerals and solid solutions, data from geochemical and geophysical studies need to be integrated into a self-consistent model.

There are two thermodynamic approaches to obtain self-consistent information on the constitution of a planet. The first one consists of a forward modelling–computer simulation of phase diagrams [27,30–32]. This approach, in which standard free energies, phase diagram and thermodynamic profiles of density, adiabatic bulk modulus and seismic parameter for a chosen petrological model are internally consistent, was applied for testing the mineral and seismic structure of the Earth's and lunar mantle [26,33–35]. The question whether phase transformations alone are sufficient or whether additional changes in chemistry are required for explanation of the nature and sharpness of the global seismic discontinuities in the Earth's mantle has been also discussed. It has been suggested that equilibrium phase changes in pyrolite within the simplified FeO–MgO–SiO_2 system cannot explain the nature of the 650-km discontinuity since the jump in seismic parameter across the discontinuity in the seismic models is 2–3 times larger than in a pyrolitic model [26]. However, a three-oxide system is oversimplification for the mantle chemistry. Further development of this approach, based on the concept of fundamental thermodynamic principles in application to planetary mantles, was outlined in [36–38]. The second approach to modelling the composition and thermal state of a planetary body consists of translating the observed seismic velocity profiles into self-consistent temperature profiles and/or bulk composition models (inverse modelling) [10,39]. A similar approach is used in a forthcoming publication (A. Khan, J.A.D. Connolly, J. Maclennan and K. Mosegaard, Selenological tomography — inferring the composition of the Moon from a Markov chain Monte Carlo inversion of the Apollo lunar seismic data, mass and moment of inertia, Geophys. J. Int.), in which the chemical composition and thermal state of the Moon is inferred by inverting the Apollo lunar seismic data set, lunar mass and moment of inertia.

The goal of this paper is to assess the mantle temperatures beneath the Archean Kaapvaal craton from both compressional and shear wave seismic velocities. For a thermal interpretation, it is necessary to know absolute seismic velocities [8,14,16]. To place constraints on the temperature distribution in the continental lithospheric mantle, we calculated a family of geotherms, making various assumptions regarding the chemical composition of the mantle. Since no attempt was made to estimate ranges of geotherms, permitted by absolute seismic velocities beneath the Kaapvaal craton, we use recent P- and S-wave models of the deep structure of the southern African region. We examine how compositional and thermal models match the seismic

data for the cratonic upper mantle. For a comparison of thermal regime of cold cratonic mantle with average normal upper mantle, it is instructive to use the IASP91 reference Earth model [40].

The first major goal is to estimate the simultaneous effect of various parameters (variations in chemical composition, pressure and temperature) on phase composition and calculate the range of seismic velocities and densities for low-temperature and high-temperature garnet peridotites at P–T conditions prevailing in the upper mantle (forward modeling) consistent with the thermochemical and elastic properties of minerals. The focus in the forward modeling is (1) to convert potentially possible bulk composition models into mineral assemblages that would be stable under the relevant ranges of pressures and temperatures, (2) to calculate the allowed seismic velocities (and densities), and (3) to compare them with seismic models. Second approach consists of converting the observed P- and S-wave velocities into temperatures. Thus, our second major aim is to retrieve the temperature distribution models for the Kaapvaal cratonic mantle from the absolute seismic velocities (inverse modeling) and to compare them with P–T estimates from mantle xenoliths and thermal models. It appears that the problems of modeling mineral composition and assessing the thermophysical properties (temperature, velocity and density distribution) of the deep interior are intimately related. Solving them simultaneously will result in the construction of a qualitatively new self-consistent petrological–geophysical model for the continental upper mantle.

2. Data and method

2.1. Thermodynamic approach

The thermodynamic properties of the Earth's interior are functions of pressure, temperature, composition and mineralogy. The crucial question is whether mantle material with velocities derived from seismic studies can satisfy both the velocities calculated from geochemical models based on xenolith data and temperatures calculated from thermal models. Phase diagrams for the FeO–MgO–SiO_2, FeO–MgO–Al_2O_3–SiO_2 and CaO–FeO–MgO–Al_2O_3–SiO_2 systems were constructed for the Earth's and lunar mantles and their topologies for various compositions were examined [26–28,33,37]. Although phase diagrams provide the basis for understanding the mineral composition of the mantle, they tell us nothing about velocities and density. The opposite is also true; seismic velocities calculated from known mineralogies [11,12,16,19,22,41] are not internally consistent with phase diagrams and cannot explain the nature and sharpness of the global seismic discontinuities in the Earth's mantle. In a strict sense, such calculations will violate basic thermodynamic principles [38].

Our approach to thermodynamic self-consistency relates equilibrium phase relations in a multicomponent system and the equations of state of minerals with seismic properties. Calculations of solid-state reactions are very sensitive to the small changes in the enthalpy, entropy and volume, and therefore the effects of heat capacity, thermal expansion and compressibility should be taken into account. The multicomponent and multiphase equilibrium calculations are best performed by adopting the method of minimization of the total Gibbs free energy (i.e., the stable phase assemblage must be determined by the lowest total Gibbs free energy of the system at a chosen chemical composition, pressure and temperature) [42], extended for calculation of phase diagrams at high pressures and temperatures [36,37]. The total Gibbs free energy of a chemical system can be expressed as:

$$G(P,T,\vec{n}) = \sum_{i=1}^{N} n_i \mu_i(P,T), \quad (1)$$

where n_i is the number of moles. Chemical potential and activity are interrelated by the expression:

$$\mu_i = \mu_i^o + RT\ln a_i = \mu_i^o + RT\ln\gamma_i + RT\ln X_i,$$

where μ^0 denotes the standard state potential, R is the gas constant, a is the activity in solution, γ is the activity coefficient, and X is the mole fraction.

The phase composition and physical properties of the mantle were modeled within the Na_2O–TiO_2–CaO–FeO–MgO–Al_2O_3–SiO_2 (NaTiCFMAS) system including the non-ideal solid solution phases: olivine (Ol), spinel (Sp), plagioclase (Pl) and ilmenite (Ilm)-binary solutions; garnet (Gar: almandine, pyrope, grossular); orthopyroxene (Opx: $MgSiO_3$, $FeSiO_3$, $Ca_{0.5}Mg_{0.5}SiO_3$, $Ca_{0.5}Fe_{0.5}SiO_3$, Al_2O_3); clinopyroxene (Cpx: same components as in Opx plus jadeite end-member). Chemical reactions in this system are independent of oxygen fugacity. We include TiO_2 in the ilmenite phase but exclude some minor elements as less significant for seismic properties of the deep interior. Since there is only restricted experimental information available on Cr-bearing garnets, these phases are not included in this study. However the influence of Cr on thermodynamic and physical properties of Cr-bearing garnet will be estimated in Section 4. The model of Stixrude and Lithgow–Bertelloni [38] is self-consistent, but phase

equilibria and velocities are computed in a simplified CFMAS system and most of their results are based on a potential temperature of 1600 K. The benefit of the more complex system is to provide the reasonable constraints on mantle chemistry. Addition of Na_2O, Al_2O_3 and Cr_2O_3 is important for stability of garnet and clinopyroxene.

2.2. Equation of state

The thermal equation of state (EOS) relates the experimental and theoretical variables, and is necessary for analysis of any thermodynamic property [43]. Here, the potential method for constructing the equation of state for solids, written in a Mie–Grüneisen–Debye form (quasi-harmonic approximation), has been used [32]:

$$P(x,T) = P_p(x) + \frac{\rho_o \gamma(x)}{x} E_T(x,T), \tag{2}$$

$$E_T(x,T) = \frac{RT}{\mu}\left[\frac{9\Theta}{8T} + 3D(\Theta/T)\right], \tag{3}$$

$$P_p = Ax^{-2/3} e^{b(1-x^{1/3})} - Kx^{-4/3}, \tag{4}$$

where E_T is the thermal constituent of internal energy in the Debye approximation, P_p is the potential constituent in the Born–Mayer form, A, b and K are the potential parameters, γ is the Grüneisen parameter, ρ is density and $x=\rho_o/\rho(P,T)$. The following constants should be set for each mineral under normal conditions (10^5 Pa, 298.15 K): adiabatic bulk modulus (K_S) and its pressure derivative, heat capacity (C_P), Debye temperature (Θ), mean atomic weight (μ), thermal expansion (α), and density.

2.3. Velocities and density of phase assemblages

At fixed P–T conditions, the high-pressure–high-temperature equilibrium phase assemblages and thermodynamic profiles of density, adiabatic bulk modulus and seismic parameter ($\Phi_s = K_s/\rho = V_P^2 - 4/3V_S^2$, where K_s and ρ are found from the equation of state) for a chosen bulk composition model are internally consistent. Isotropic velocities of P- and S-waves for mantle composites have been found from the relations:

$$V_P(P,T,X) = \{(K_s + 4/3G)/\rho\}^{1/2}, V_S(P,T,X) = \{G/\rho\}^{1/2}$$

For the shear modulus we assume a linear dependence on pressure and temperature:

$$G(P,T) = G(P_o,T_o) + (\partial G/\partial P)(P-P_o) + (\partial G/\partial T)(T-T_o) \tag{6}$$

The Hill average of the Voigt and Reuss bounds was used for estimating the theoretical velocities for the equilibrium assemblage of a given chemical composition. These velocities, which take into account phase transformations of a multiphase equilibrium assemblage as well as anharmonic effects, are compared with seismic observations for the Kaapvaal craton. The effects of anelasticity and anisotropy on seismic velocities, and sensitivity of density and velocities to temperature, pressure and composition are discussed in 2.4, 3.1 and 4.1, 4.2, 4.3.

2.4. Calculation of mantle temperatures from seismic velocities

Temperature dependence of seismic velocities comes both from anharmonicity and anelasticity; the latter is an important effect at seismic frequencies [44]. Strong effect of temperature on seismic velocities and attenuation is well-known from experimental studies [45,46]. Following many authors [14,16,44], anelastic effects must be included for comparing theoretical velocities with geophysical interpretations:

$$Q_S(P,T,\omega) = A\omega^{\alpha}\exp(\alpha E^*/RT), E^* = H^* + PV^*,$$

$$Q_P^{-1} = (1-L)Q_\kappa^{-1} + LQ_S^{-1}, \tag{8}$$

where Q_S ($Q_S = Q_\mu$) and Q_P are S- and P-wave quality factors, a scaling constant $A=0.148$, E^* is the activation energy ($H^*=500$ kJ/mol, $V^*=20$ cm^{-3} mol), $\alpha=0.15$, ω is wave frequency, $L=4/3(V_S/V_P)^2$, Q_K is bulk waves quality factor defined here as $Q_K = Q_{K,100\ km}(Q_S/Q_{S,100\ km})^{1.5}$, where $Q_{K,100\ km}=1000$; under this condition the Q_P/Q_S ratio is maximal and equal to $1/L$, and $Q_P < Q_S/L$ [47].

Velocity, with account for both anharmonic and anelastic effects, can be expressed as:

$$V(P,T,X,\omega) = V_{anh}(P,T,X)[1-1/2Q_{P,S}(P,T,\omega)\tan(\pi\alpha/2)], \tag{9}$$

where X stands for the bulk composition model and $V_{anh}(P,T,X)$ are self-consistent anharmonic P- and

S-velocities calculated from Eqs. (1)–(6) for each equilibrium phase assemblage. Calculations were performed for $f=0.1$ Hz. Retrieving the temperature distribution from seismic models is based on minimizing the deviations between calculated and observed seismic velocities. The derived temperature profiles are not sensitive to the starting temperature. Our numerical experience has shown that after 10–20 iterations we can determine the temperature distribution with depth corresponding to the equilibrium phase assemblage and seismic velocities with the uncertainty not greater than 1 °C. The pressure–depth correlation was taken from the reference Earth model (PREM).

2.5. Geochemical constraints

The great majority of mantle xenoliths are peridotites [48–52]. Studies of peridotites from kimberlites indicate that cratonic mantle is strongly depleted in basaltic components. The pressure–temperature conditions of equilibration of garnet peridotites from the Kaapvaal craton fall into two main P–T regions, representing a low-temperature and a high-temperature group [48]. Low-T coarse garnet peridotites have been interpreted as representing samples from the lithospheric mantle, originating from depths < 150 km, whereas sheared or deformed high-T peridotites have been interpreted as representing asthenospheric samples from depths greater than 150–175 km, but which are now considered to be metasomatized samples of highly depleted Archean mantle [22]. According to [53], the depleted mantle roots beneath continental cratons would represent the refractory relicts of a Si- and Fe-rich Early Archean mantle.

The P–T conditions of equilibration of garnet-bearing lherzolite xenoliths from kimberlite localities within the Kaapvaal craton (Bultfontein, Jagersfontein, Monastery, and Premier) were estimated using three sets

Table 1
Bulk composition models (wt.%), phase composition (mol%) and physical properties of garnet peridotite xenoliths, average garnet peridotite (GP) and primitive mantle (PM) composition[a]

Composition	JAG90-10	JAG90-11	PR90-57	JAG90-13	JAG90-19	PR90-9	GP	GP	PM	PM
SiO_2	42.96	46.98	45.52	47.74	43.64	44.88	45.42	45.42	45.25	45.25
TiO_2	0.10	0.07	0.07	0.07	0.05	0.10	0.08	0.08	0.21	0.21
Al_2O_3	0.36	1.69	2.19	1.35	1.37	2.11	1.32	1.32	4.50	4.50
FeO	6.48	6.31	7.56	7.13	7.50	7.96	7.03	7.03	8.48	8.48
MgO	49.38	43.93	42.14	42.25	46.29	42.83	45.28	45.28	37.58	37.58
CaO	0.49	0.78	2.19	1.20	0.94	1.90	0.78	0.78	3.64	3.64
Na_2O	0.23	0.24	0.33	0.26	0.21	0.22	0.09	0.09	0.34	0.34
Total	100	100	100	100	100	100	100	100	100	100
MG#	93.15	92.53	90.85	91.37	91.66	90.55	92.00	92.00	88.8	88.80
Phase composition, physical properties										
H (km)	125	125	125	175	175	175	125	175	125	175
P (GPa)	3.95	3.95	3.95	5.6	5.6	5.6	3.95	5.6	3.95	5.6
T (°C)	1000	1000	1000	1300	1300	1300	1000	1300	1000	1300
Ol	85.5	55.5	61.7	49.8	78.3	65.8	65.5	65.6	55.4	55.5
Gar	0.4	1.3	1.8	0.8	1.2	2.1	1.3	1.4	5.1	5.2
Opx	10.7	34.5	13.8	37.5	8.5	11.8	26.9	26.9	2.5	0.0
Cpx	3.2	8.6	22.6	11.8	11.9	20.1	6.2	6.0	36.6	38.9
Ilm	0.2	0.1	0.10	0.1	0.1	0.2	0.1	0.1	0.4	0.4
ρ (g cm^{-3})	3.290	3.304	3.331	3.318	3.323	3.343	3.311	3.317	3.381	3.389
V_P (km s^{-1})	8.319	8.246	8.244	8.225	8.316	8.284	8.259	8.290	8.271	8.308
V_S (km s^{-1})	4.640	4.632	4.599	4.556	4.567	4.552	4.622	4.574	4.591	4.550

[a] Bulk compositions of garnet peridotite xenoliths normalized to 100% were taken from Grégoire et al. [54]; phase composition, V_P, V_S, and density are calculated at P–T conditions of equilibration. JAG = Jagersfontein, PR = Premier; JAG90-10, JAG90-11 and PR90-57 — coarse; JAG90-13, JAG90-19 and PR90-9 — deformed; MG# 100Mg/(Mg+Fe) — molar.

Average bulk composition of garnet peridotite (GP) [51]; GP phase composition (mol%) at 3.95 GPa and 1000 °C: 65.5% Ol ($Fo_{92.5}$) + 1.3% Gar ($Py_{82}Alm_{15}Gros_3$) + 26.9% Opx ($En_{89}OrthoDi_2OrthoFs_{7.4}OrthoHed_1OrthoCor_{0.6}$) + 6.2% Cpx ($ClEn_{36.6}Di_{31.6}ClFs_{5.5}Hed_{12}Jd_{13}ClCor_{1.3}$) + 0.1% Ilm ($Geik_{65}$); GP phase composition at 5.6 GPa and 1300 °C: 65.6% Ol ($Fo_{92.4}$) + 1.3% Gar ($Py_{85}Alm_{12}Gros_3$) + 0.1%Ilm($Geik_{74}$) + 27% Opx ($En_{88}OrthoDi_3OrthoFs_{7.2}OrthoHed_{1.2}OrthoCor_{0.6}$) + 6.0% Cpx ($ClEn_{42}Di_{27}ClFs_5Hed_{12}Jd_{13}ClCor_1$).

Bulk composition of primitive mantle (PM) from [51]; phase composition (mol%) at 5.6 GPa and 1300 °C: 55.5% Ol (Fo_{91}) + 5.2% Gar ($Py_{82}Alm_{14}Gros_4$) + 38.9% Cpx ($ClEn_{40}Di_{31}ClFs_6Hed_{14}Jd_8ClCor_1$) + 0.4% Ilm($Geik_{68}$).

of geothermobarometers [54]. Olivine and orthopyroxene are the main mineral constituents of these rocks [52,54]. Other lithologies that occur in the upper mantle are significantly less abundant than peridotites. Here we restrict our analysis to some of these xenoliths and use the average composition of garnet peridotite (hereafter

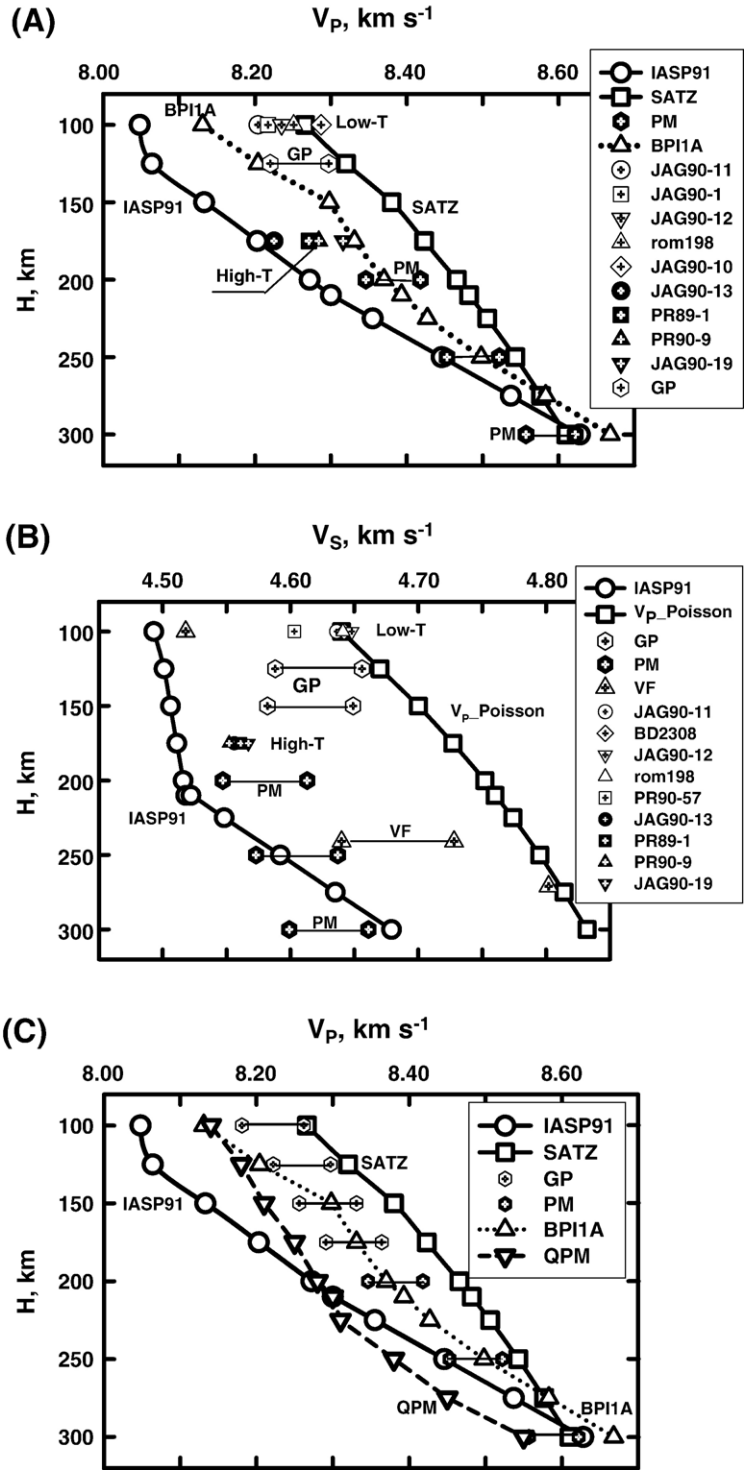

GP model) determined from 24 southern African garnet peridotite xenoliths [51]. We approximate the composition of the "asthenosphere" by primitive mantle composition (PM model) of McDonough [51], which is close to the pyrolite composition. Phase compositions and physical properties calculated for several compositional models are listed in Table 1. Kaapvaal GP compositions have higher Mg numbers and are low in Al and Ca, and garnet and clinopyroxene compared to the primitive mantle. Kaapvaal peridotites are depleted in FeO and Al_2O_3, leading to low intrinsic density.

2.6. Seismic constraints

P- and S-wave tomographic results show that a high-velocity lithosphere root extends beneath the Kaapvaal craton to a depth of ~250 km [55]. Three-dimensional seismic images of P- and S-velocity structure beneath southern Africa, based on analysis of the Kaapvaal data, suggest that seismic velocities are 0.5–1% higher than those in the off-craton upper mantle [22,55]. Despite lack of evidence of a low-velocity zone (LVZ) in the cratonic mantle was found either from body- or surface wave analyses [55–61], the presence of a LVZ was suggested in [62–65]. However, its depth and the very existence remain enigmatic. In general, velocity reduction can be caused by the transition from depleted to metasomatised lithosphere or by a small amount of partial melt [66–68]. According to [64], the LVZ in model BPISM appears to be located outside the craton (i.e., on the cratonic margins and adjacent mobile belts) and may be associated with temperature gradients alone without partial melting.

We focus on the upper mantle under the Kaapvaal craton for which absolute seismic velocities are available. Zhao et al. [56] investigated the upper mantle seismic velocity structure, using travel time and waveform data, constrained by a large mine tremor in South Africa recorded by the Tanzania broadband seismic experiment. Their S-wave velocity model (model V_p–Poisson) was constructed using the SATZ model and assuming a constant Poisson's ratio of 0.27. Travel times from earthquakes recorded at stations of the Kaapvaal and South African National networks were used to derive an average P velocity model (BPI1A) for the upper mantle below and around the Kaapvaal craton at depths down to 800 km [57]. We inverted for temperature the recent P and S velocity models of Zhao et al. [56], Qiu et al. [62], Simon et al. [57], and Vinnik and Farra [60] as well as the IASP91 reference Earth model [40].

2.7. Input data and method of solution

By applying suitable thermodynamic models for the equation of state of minerals and solid solutions and the technique of free energy minimization, phase relations, seismic velocities and density can be derived entirely from an internally consistent model, with only thermodynamic data and bulk composition as input. The bulk composition (unless noted otherwise) is assumed to be fixed with depth whereas the phase composition, phase proportions and chemical composition of the coexisting phases are changing with pressure and temperature (Table 1). Input data for the self-consistent thermodynamic quantities (enthalpy of formation, entropy, heat capacity, and Margules parameters for non-ideal solid solutions), for the EOS of minerals as well as for shear moduli and their derivatives are summarized in the THERMOSEISM data base [69], which includes a series of computer codes for both forward and inverse solutions of the problem of mantle structure. The THERMOSEISM data base was established by supplementing the calorimetric data for low-pressure phases and the EOS for low- and high-pressure phases with data calculated from high-pressure experiments [33,36, 39,69]. Forward code calculates the equilibrium phase assemblages and their velocities and densities. Inverse code computes the temperature distribution in the mantle from seismic and compositional constraints. Anharmonic and anelastic effects are taken into account. The output results contain the self-consistent information on phase assemblages,

Fig. 1. Comparison of P- and S-velocities (calculated only from the anharmonic part of seismic velocities) for low-T (coarse) and high-T (deformed) xenoliths from the Kaapvaal craton, average composition of garnet peridotite (GP) at depths of 100–175 km and primitive mantle composition (PM) at greater depths with the IASP91 reference model [40] and seismic models for southern Africa: QPM (Qiu et al. [62]), VF (Vinnik and Farra [60]), BPI1A (Simon et al. [57]), SATZ and model V_p–Poisson (Zhao et al. [56]). Velocities for the GP and PM phase assemblages are calculated with the temperature variations of ±100 °C (Appendix, Table A). P- and S-velocities for low-T and high-T xenoliths are calculated (within the P–T conditions of equilibration [54]) at 900 °C and 100 km depth, and at 1300 °C and 175 km depth, respectively. (A) P-velocities for low-T xenoliths (8.20–8.29 km s^{-1} at 100-km depth and 900 °C) are between the SATZ and BPI1A velocities, whereas P-velocities for high-T xenoliths (8.225–8.316 km s^{-1} at 175-km depth and 1300 °C) are slower than seismic velocities [56,57] at the same depth; (B) S-velocities for the GP and PM models and xenoliths; S-velocity profile in the VF model [60] shows a sharp increase in velocity at 241 km depth from 4.64 to 4.728 km s^{-1}, $\delta V/V_S$=1.9% (L.Vinnik, personal communication); (C) P-velocities for the GP and PM models in comparison with seismic models. The wavespeeds of BPI1A to 270-km depth lie between those of the SATZ model and the IASP91 model. At a depth of about 270–300 km, some of the seismic models converge.

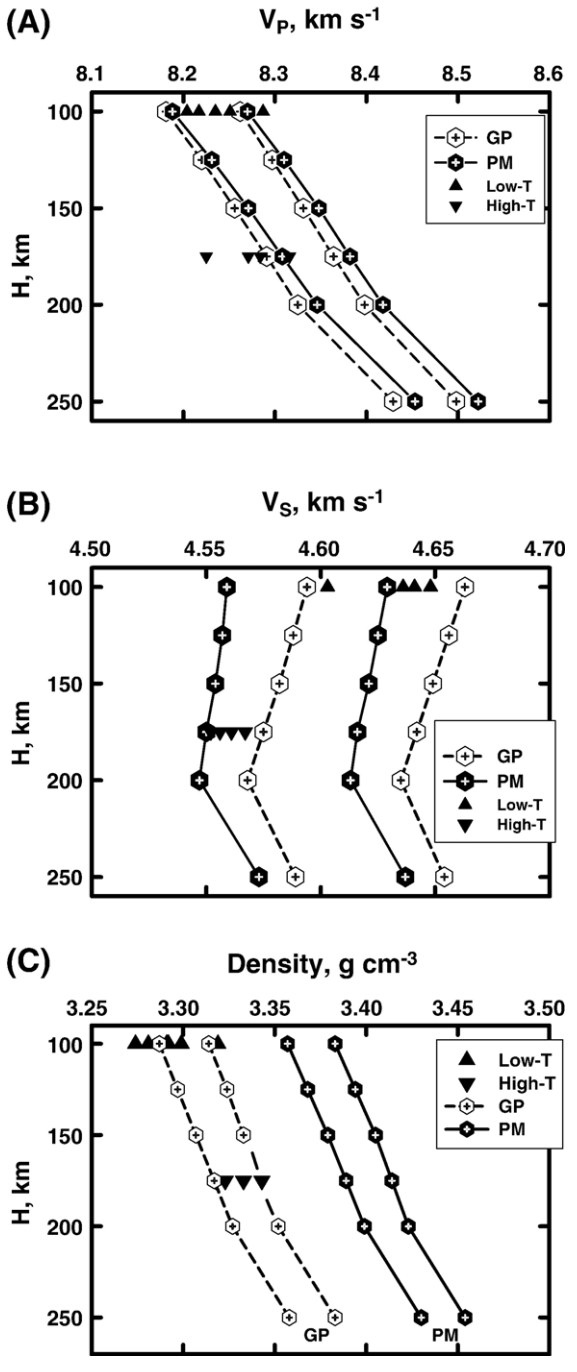

Fig. 2. Comparison of anharmonic P-velocities (A) and S-velocities (B), and densities (C) for low-T and high-T xenoliths, depleted garnet peridotite (GP) and primitive mantle composition (PM). For the GP and PM models, velocities and densities are calculated with the temperature variations of ±100 °C at each depth (Table A). P- and S-velocities and densities for low-T and high-T xenoliths are calculated (within the P–T conditions of equilibration [54]) at 900 °C and 100 km depth, and at 1300 °C and 175 km depth, respectively. PM composition is 0.07 g cm^{-3} denser that GP composition.

densities and velocities. This is a very important aspect of the present work, not considered by other authors in modeling the constitution of the Earth's mantle. The approach used here requires a small number of thermodynamically defined parameters and has important advantages over earlier procedures, which contain no information about entropy, enthalpy and Grüneisen parameter.

3. Results and discussion

3.1. Sensitivity of density and velocities to temperature, pressure and composition

At a given chemical composition, seismic velocities and densities depend on variations in pressure, temperature and on the phases stable at various depths of the mantle. An important issue is to estimate the simultaneous influence of various parameters (variations in chemical and phase composition, pressure and temperature) on physical properties. Velocities and densities as a function of depth are calculated for the depleted garnet peridotite (GP model) and non-depleted primitive mantle composition (PM model), and for the garnet lherzolite xenolith samples from their bulk chemical compositions at equilibration pressure and temperature [54] (Figs. 1 and 2, Tables 1, 2 and Table A in Appendix).

Our results for the GP model indicate an upper mantle mineralogy as consisting chiefly of olivine (65.5 mol%, $Fo_{92.5}$), two aluminous pyroxenes (27 mol% Opx and 6 mol% Cpx) and garnet (1.3 mol%) down to about 290–300 km depth, where the two pyroxenes are replaced by a single high-pressure clinopyroxene, and trace amounts of ilmenite. At 10 GPa (~300 km) and 1400 °C, this phase transformation is accompanied by a jump in density and velocities in agreement with the acoustic measurements [70]. The expected location of this phase transition probably coincides with a small magnitude seismic discontinuity, the "X-discontinuity", occasionally observed in seismic profiles at a 300 km depth [71,72]. Phase proportions of the same phase assemblage vary sufficiently with changes in bulk composition (Table 1). For example, olivine content varies from 50% (JAG90-13) to 85% (JAG90-10) whereas orthopyroxene content varies from 8.5% (JAG90-19) to 37.5% (JAG90-13). At depths of 175–300 km, the fertile PM composition consists essentially of olivine (56 mol%, Fo_{91}), aluminous Cpx (38 mol%) and garnet (5–6 mol%). These variations influence the calculated velocities and densities (Figs. 1 and 2).

The effect of chemical composition and temperature on the physical properties of cratonic mantle in

Table 2
Physical properties of low-T (JAG90-10, JAG90-11, PR90-57) and high-T (JAG90-13, JAG90-19, PR90-9) xenoliths (Kaapvaal Craton) calculated at the P–T conditions of equilibration [54]

Physical properties	JAG90-10	JAG90-11	PR90-57	JAG90-13	JAG90-19	PR90-9
P (GPa)/T (°C)	3.8/946	2.5/712	2.9/927	4.6/1231	4.9/1283	4.5/1275
	4.3/1076	3.4/708	4.4/1101	5.8/1264	5.7/1351	5.1/1296
	4.2/942	3.2/900	2.9/920	5.8/1306	5.6/1308	6.1/1371
ρ (g cm^{-3})	3.295	3.300	3.310	3.298	3.306	3.315
	3.291	3.327	3.330	3.328	3.319	3.329
	3.306	3.295	3.311	3.323	3.322	3.347
V_P (km s^{-1})	8.326	8.222	8.170	8.157	8.263	8.194
	8.319	8.308	8.246	8.257	8.305	8.241
	8.360	8.214	8.173	8.241	8.313	8.301
V_S (km s^{-1})	4.656	4.679	4.586	4.544	4.550	4.522
	4.627	4.710	4.580	4.575	4.552	4.536
	4.669	4.640	4.588	4.561	4.564	4.544

comparison with the IASP91 model [40] and seismic models for southern Africa [56,57,60,62] is shown in Fig. 1. As there is no a priori temperature profile, P- and S-wave velocities and densities for the GP and PM models are calculated in a wide temperature range from 800–1000 °C at 100 km depth to 1200–1400 °C at 200 km depth, and to 1300–1600 °C at 250–300 km depth (see Table A in Appendix) in agreement with xenolith P–T estimates [54] and thermal models for Archean regions [1,4]. Calculated velocities are between the fastest and slowest seismic models reported for southern Africa.

Figs. 1 and 2 compare the density and velocity values for low-T (coarse) and high-T (deformed) xenoliths (calculated within the P–T conditions of equilibration [54]) with those for the petrologic and seismic models. Variations in chemical composition and phase proportions of xenoliths (Table 1) have appreciable influence on velocities and densities of cratonic mantle. Variations in phase proportions of low-T and high-T xenolith samples exhibit a range of 1% in P-velocities (Fig. 2A), 0.3–1% in S-velocities (Fig. 2B), and 0.7–1.4% in density (Fig. 2C). For the average GP model and cratonic xenoliths, the ranges of densities and velocities at 100 and 175 km depth are close to those plotted in Figs. 4 and 6 in James et al. [22]. The discrepancies of geothermobarometry calculations reach 200 °C and 0.5–1.5 GPa [54]. The composition-induced velocity and density contrasts are equivalent to those that could be produced by temperature and pressure contrasts of 100–200 °C and 1 GPa (Table 2). This is significantly less than seismic discrepancies at depths between 100 and 200 km (Fig. 1). The seismic velocity contrasts must lead to the significant temperature contrasts.

For the PM model, P- and S-velocities are estimated to be 8.35–8.42 and 4.55–4.61 km s^{-1} at 200 km depth, and 8.45–8.52 and 4.57–4.64 km s^{-1} at 250 km depth (Fig. 2A,B). It is important to note that at the same P–T conditions, the PM composition has significantly higher density than the GP composition ($\Delta\rho/\rho \approx 2\%$, Fig. 2C) but comparable velocities: P-velocities for the PM are slightly greater ($\leq 0.4\%$) than those for the GP, whereas S-velocities for the PM are slightly less ($\leq 0.6\%$) than those for the GP (Fig. 2A,B). It means that P- and S-velocities for depleted and fertile compositions are not sufficiently different. Thus, a change of composition from depleted garnet peridotite to fertile primitive mantle shows minor effects on the velocities. This conclusion contradicts the calculations of James et al. [22] and Kuge and Fukao [19] who found that P- and S-velocities for fertile garnet peridotite are consistently lower (by 1–1.5% [22]) relative to the Kaapvaal garnet lherzolites and depleted composition model of the Archean lithosphere.

It is commonly accepted that temperature is the main parameter affecting seismic velocities in the mantle [16,18]. Indeed, Fig. 2 shows that velocities for both the GP and PM models are more sensitive to temperature than to composition. Note, however, that composition has a complex effect on densities and velocities: an increase in the FeO content and a decrease in the Al_2O_3 content lead both to a velocity decrease but can compensate a change in density [73]. For a given chemical composition, the effect on density of temperature variations of ±100 °C is not greater than ±0.014 g cm^{-3} (±0.4%), Table A.

However, density is more sensitive to composition than to temperature (Fig. 2C). Compositional gradients from depleted to fertile material lead to a significant change in density ($\Delta\rho/\rho = 2.1\%$), resulting in only minor changes in both velocities (~0.5%). At a depth of 200 km, this density variation translates to an

uncertainty in temperature of ±300 °C. Thus, composition-induced density variations are sufficiently high in terms of corresponding temperature. The garnet peridotite has a calculated density of 3.35–3.33 g cm^{-3} at 6.45 GPa (~200 km) and 1200–1400 °C, which is significantly less than primitive mantle (3.42–3.4 g cm^{-3}). Even a relatively more fertile xenolith sample, PR90-9, is lower in density (ρ(4.5–6.1 GPa/1275–1371 °C)=3.315–3.35 g cm^{-3}) in comparison with the PM composition (ρ(5.6 GPa/1300 °C)=3.39 g cm^{-3}), see Tables 1 and 2. Such a decrease in density will stabilize the old cratonic lithosphere [21].

3.2. Temperature profiles from P- and S-wave velocities

A set of geotherms for the depleted and fertile upper mantle beneath the southern Africa (Kaapvaal craton) and "normal" mantle (i.e., average continental mantle), inferred from seismic observations, is shown in Fig. 3. The bulk composition (but not the phase composition

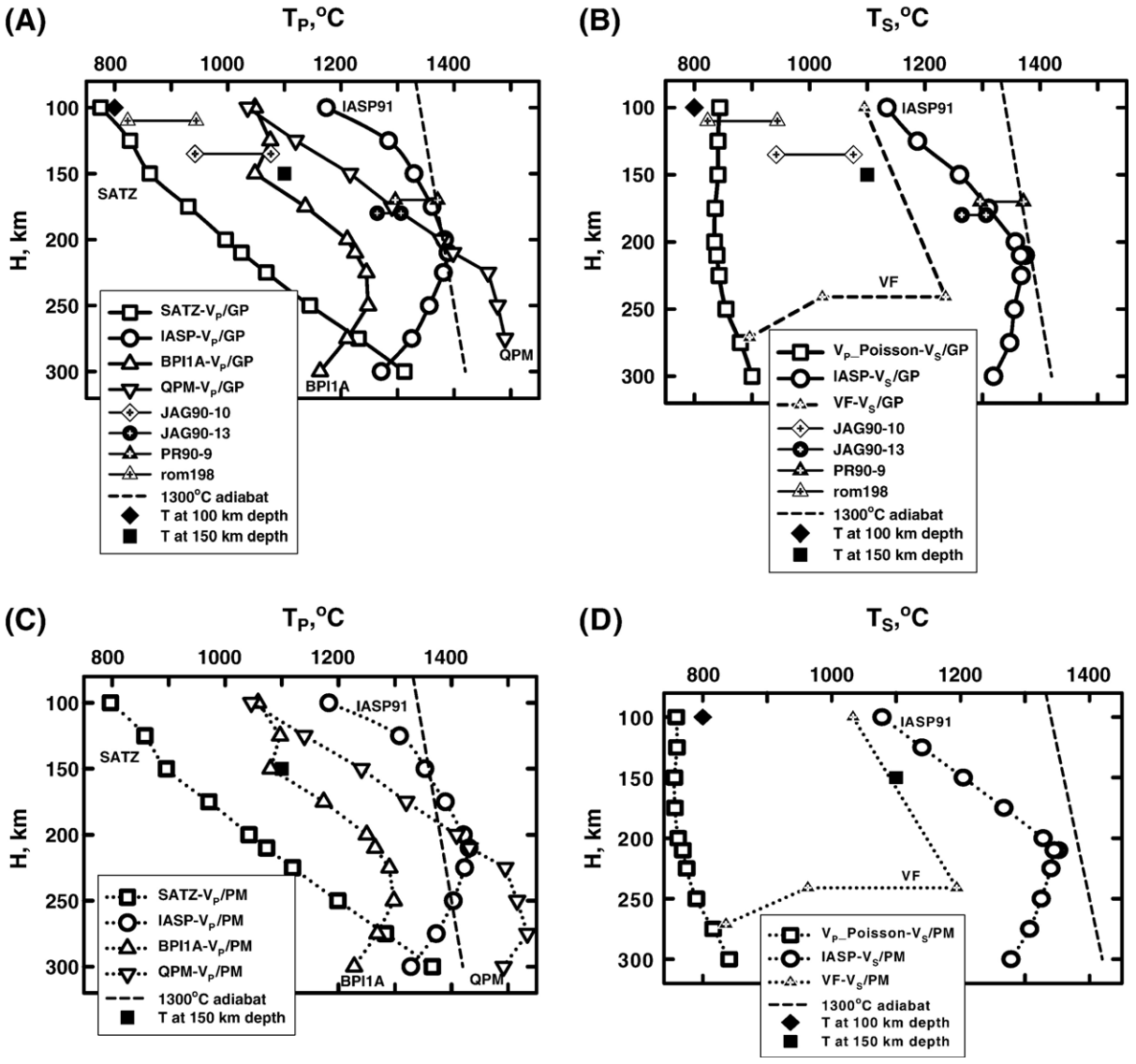

Fig. 3. Estimation of upper mantle temperatures from seismic and geochemical constraints. T_P and T_S are temperatures inferred from P- and S-wave velocities for the GP (A, B) and PM (C, D) compositions. Calculated temperatures include both anelastic and anharmonic effects in the seismic velocities. Definitions of seismic models are given in Fig. 1. Temperatures inferred from the IASP91, BPI1A, QPM and VF models display an inflection at depths greater than 210 km, leading to a non-physical behavior of geotherms. Estimated temperatures at 100 and 150 km depth [1] and xenolith *P–T* points [54] are shown. The 1300 °C adiabat with a plausible adiabatic gradient of 0.4 °C/km is shown by a dashed curve.

and phase proportions) is assumed to be fixed with depth (Table 1). T_P and T_S are temperatures inverted from P- and S-wave velocities for the GP (Fig. 3A,B) and PM (Fig. 3C,D) models. Widely variable temperature profiles are obtained, depending on the seismic velocity values. Note that relatively small variations in velocities (~1% in V_P) correspond to large temperature variations (~15–20% or ΔT~170 °C).

Let us consider first the cratonic mantle composed of the GP assemblage that appears to be both more refractory and colder than the surrounding asthenospheric mantle. T_P and T_S data for the GP model show a considerable difference. Velocity contrasts lead to a temperature contrast of ~300 °C. At a depth of 100 km, temperatures range from T_P=775 °C and T_S=845 °C for the fastest SATZ and V_p–Poisson models [56], derived over a region extending north from the Kaapvaal craton to the Tanzanian craton, to T_P=1050 °C for the BPI1A model [57] beneath the Archean core of southern Africa, to T_P=1035 °C for the QPM model [62], and to T_S=1095 °C for the VF model [60] (Fig. 3a,b). On the whole, minimum and maximum $T_{P,S}$ under the craton at 100–150 km depth are between 800 °C and 1100 °C, in general agreement with the P–T estimations for the coarse garnet lherzolites [54] and thermal models [1,74] (Fig. 3). According to Grégoire et al. [54], the P–T estimations for the deformed samples from Jagersfontein and Premier (JAG90-13, JAG90-19, PR89-1, PR90-9) range from 1250 to 1350 °C at 160–190 km depth. Equilibration temperatures for these high-T deformed samples are close to $T_{P,S}$ derived from the IASP91 model and a mantle adiabat but are 300–500 °C higher than $T_{P,S}$ estimated from the fastest SATZ and V_p–Poisson models [56] (Fig. 3A,B).

The IASP91 model shows low wavespeeds compared with regional seismic models for the Kaapvaal craton (Fig. 1). Therefore, T_P and T_S derived for the normal mantle from the IASP91 model are much higher than those from regional models. In contrast to temperatures from regional models, seismic temperatures, inferred from the IASP91 model, agree rather well with each other. At a depth of 100 km, T_S=1135 °C and T_P=1175 °C for the GP composition, and T_S=1080 °C and T_P=1180 °C for the PM composition (Fig. 3). At depths between 100 and 300 km, the differences between T_P and T_S for the GP and PM models are as follows: T_P (GP) is 10–40 °C lower than T_P(PM) while T_S (GP) is 30–60 °C higher than T_S(PM).

The slowest regional QPM model [62] results in a hottest temperature profile with T_P of 1380–1520 °C at depths of 200–250 km (Fig. 3A,C), which intersects a 1300 °C mantle adiabat at ~200 km depth. In the revised model of Priestley [63] the minimum value of S-velocity (4.45 km s^{-1}) at depths of 200–250 km translates to temperature as high as 1430–1590 °C. For a comparison, from the IASP91 model: T_S(210 km)= 1340–1370 °C and T_P(210 km)=1390–1430 °C for both GP and PM models.

At a depth of 200 km, seismically permissible variations in temperature between the cratonic (SATZ and V_p–Poisson models) and normal (IASP91 model) mantle reach 380 °C for T_P and 570 °C for T_S for both GP and PM compositions. It is important to note that except for the fastest Zhao et al. velocity models, temperatures inferred from the IASP91, BPI1A, QPM and VF models display an inflection at depths greater than 210 km (Fig. 3A,B,C,D).

The Zhao et al. models [56] do not display temperature inflections and lead to the lowest lithospheric temperatures: $T_P \approx$ 800–1000 °C at depths of 100–200 km (Fig. 3a,c); T_S is nearly constant with a small negative gradient at these depths (Fig. 3B,D) and results in an unreasonable geotherm, which never intersect the mantle adiabat. At depth of 200–300 km P and S velocities [56] yield incompatible temperature estimates: temperatures from S-velocities are systematically lower than those estimated from P-velocities. The fastest SATZ model results in a coldest temperature profile with the gradient of 3 °C/km at depths of 200–275 km; this temperature profile intersects a 1300 °C mantle adiabat at depths greater than 300 km (Fig. 3A, C) and lies about 200 °C lower than a conductive geotherm for 40 mW m^{-2} surface heat flow [3].

Temperature estimates from the S-velocity profile of the VF model [60] (Fig. 3B,D) show much higher temperatures than the V_p–Poisson model [56] at 100–240 km depth. At an upper bound of a 241-km discontinuity the difference in temperature reaches 400 °C. However, just below the discontinuity a jump in S-velocity [60] leads to a dramatic decrease in temperatures from 1200–1235 °C to 960–1020 °C and to 840–900 °C at 271 km depth. Such a decrease in temperatures is produced by a strong velocity jump in the VF model, which below the 241-km discontinuity is significantly faster than the IASP91 model (Fig. 1B). For a uniform composition, the sharp velocity increase across the discontinuity ($\delta V/V_S$=1.9%) in the VF model [60] results in unrealistic temperature profiles, irrespective of the composition model. We could not explain the amount of S-wave velocity jump at a depth of 241 km.

The resulting T_P and T_S profiles inferred from the IASP91 velocities for the average continental mantle are similar. On the other hand, variations of 50–100 °C in the inferred temperatures indicate the incomplete

consistency between absolute P- and S-velocities in the IASP91 model. On the whole, we find a good agreement between T_P and T_S; Figs. 3A,B and 2C,D show that T_P and T_S are only weakly dependent on composition. Paradoxically, however, the IASP91 model, having maximal temperatures at 210 km (T_P=1390 °C and T_S=1370 °C for GP composition, and T_P=1430 °C and T_S=1340 °C for PM composition), leads to a temperature inflection with a negative temperature gradient at depths below 210 km leading to non-physical temperature behavior. The same temperature anomaly patterns in cold cratonic mantle are found for the VF and BPI1A models. Fig. 3A and C show that the temperature profiles derived from the BPI1A model, reaching the maximum temperature of 1250 °C (GP model) and 1300 °C (PM model) at a depth of 250 km, display an inflection to lower temperatures at depths>250 km; for 125–150 km depth, the change in temperature slope of unclear origin also occurs.

Alternative to a compositional interpretation of the non-physical temperature behavior can be attributed to thermodynamic and seismic uncertainties or to variations in anelasticity with depth [8,13,18,45,46]. However, since we obtain consistent temperature behavior from both the P- and S-velocity profiles, our results do not seem to be strongly biased by these effects. On the other hand, a conclusion that IASP91 seismic gradients give negative temperature gradients below about 200 km depth is consistent with [8] that mostly did not use a fully self-consistent approach. So, the inflection to low temperatures cannot be an artefact of the method of temperature determination. Negative temperature gradients inferred for normal upper mantle might indicate either a gradual change in composition or seismic uncertainties associated with an unreasonable velocity gradient. At depths of 210–300 km, seismic gradient in the IASP91 model ($\Delta V_P/\Delta H$=0.00365 s^{-1}) is higher than that in the BPI1A model ($\Delta V_P/\Delta H$=0.0031 s^{-1}) and 2.5 times greater than P-velocity gradient in the SATZ model ($\Delta V_P/\Delta H$=0.0014 s^{-1}).

3.3. Compositional effects and chemical stratification of the cratonic mantle

P- and S-velocities of all seismic models considered here increase monotonically with depth. Therefore, it is impossible to explain the kinks of geotherms, derived for the GP and PM models, by the presence of small amounts of free fluid or hydrous phases, plume-related effects or partial melt-bearing asthenosphere beneath the lithosphere [14,66,67,75], which must lower the mantle velocities. At the same time, a hypothesis of the average composition of garnet peridotite (GP model) determined from the southern African garnet peridotite xenoliths [51] is non-applicable to the upper mantle because of decreasing T_P and T_S with depth. In Fig. 4 we present the T_P estimates from the BPI1A model [57] obtained when P-velocities are inverted assuming compositional models for low-T and high-T xenoliths of the Kaapvaal craton [54]. We perform inversions with different xenolith compositions to explore the sensitivity of temperature to variations in bulk composition and mineralogy.

The effect of specific composition of garnet peridotite xenoliths on the evaluated temperatures for ten compositional models together with GP and PM models is illustrated in Fig. 4. This plot clearly shows that temperatures depend rather strongly on bulk composition and proportion of phases stable at various depths of

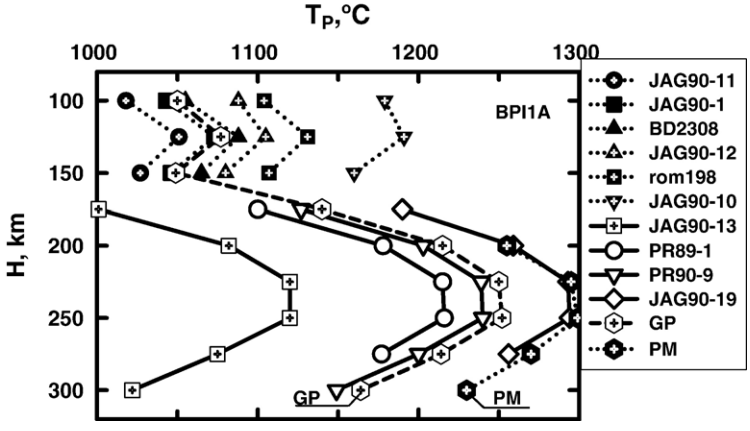

Fig. 4. Effect of specific composition of garnet peridotite xenoliths from the Kaapvaal craton on the evaluated temperatures; T_P estimates from the BPI1A model [57]. Variations in inferred temperatures reach ~200 °C for both low-T and high-T xenoliths.

the upper mantle. This implies further that lithospheric thickness (as defined by the intersection of the geotherms and mantle adiabat) depends significantly on xenolith compositions. The relatively small differences between the xenolith compositions translate into appreciable variations in inferred temperature. The evaluated temperatures differ by ~200 °C, and negative temperature gradients occur in two depth ranges. The GP model falls within the temperature range that is bounded by compositional models shown in Fig. 4. Sample JAG 90-19 with deformed texture [54] and PM model indicate similar temperatures. A change in enigmatic temperature slope at depths of 125–150 km may be attributed mainly to a high BPI1A velocity gradient at these depths or to variations in anelasticity with depth.

A set of kinks on temperature profiles accompanied by a decrease in temperature in the sufficiently cold cratonic mantle (and in the normal upper mantle) occurs at depths below ~220 km (the Lehmann discontinuity?). Nature of this discontinuity is controversial. It has been proposed that the Lehmann discontinuity can represent a change in composition or in anisotropy, a change from conductive to convecting regime, and the transition in deformation mechanism from dislocation to diffusion creep [e.g., 48,76]. A change in chemical composition, which is imperfectly known, is frequently suggested as an explanation for the Lehmann discontinuity. In Fig. 4, we show that either low-T and high-T peridotites, depleted in Fe, Al and Ca, or fertile asthenospheric material (PM model), enriched in Fe, Al and Ca, cannot explain the nature of the inflections below 220 km. The negative temperature gradient obtained from V_P (from IASP91, BPI1A and QPM models) and V_S (from IASP91 and VF models), with exception of the SATZ model and model V_p–Poisson [56], means that a fixed bulk composition is non-applicable to the upper mantle and implies a complex influence of the composition on the estimated temperatures. The transition from highly depleted low-T to less depleted high-T peridotitic mantle fails to explain the inflections of geotherms (Fig. 4).

In Fig. 5, we illustrate an influence of uniform and variable compositions on temperatures derived from three seismic models. T_P and T_S are inferred from the IASP91 [40] and Zhao et al. P- and S-velocities [56] for the GP (at 100–210 km depth) and PM (210–300 km) uniform compositions. T_P profile is inferred from the BPI1A model [57] for variable composition. Two features of this plot are particularly interesting. The first is that P and S models of Zhao et al. yield incompatible temperature estimates. As a result, T_P and T_S contrasts are highest for the cratonic mantle. Poor

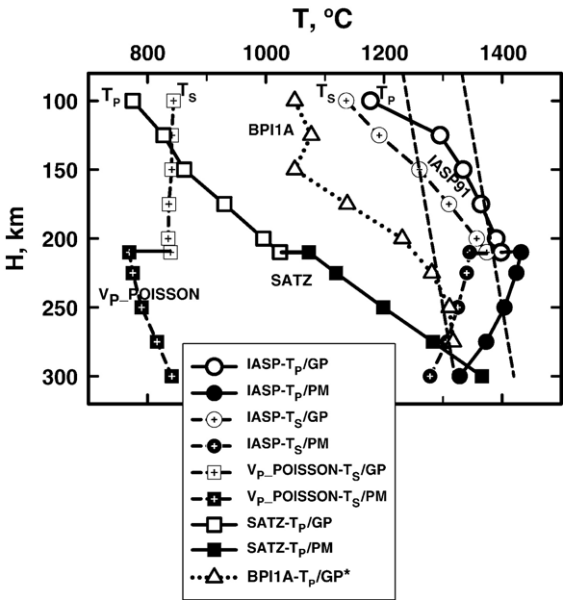

Fig. 5. T_P and T_S inferred from the BPI1A P-velocity profile [57], the IASP91 model [40] and the Zhao et al. P- and S-velocities [56]. Three composition models are used: depleted garnet peridotite (GP) at depths of 100–210 km; primitive mantle composition (PM) at depths of 210–300 km; variable bulk composition (GP*) with a gradual increase in fertility at depths between 200 and 275 km (Table 3). T_P (PM) estimated from [40,57] are higher than T_P (GP) while T_S (PM) are lower than T_S (GP). The variations in the GP* composition and phase proportions result in the monotonous temperature profile derived from the BPI1A model at 200–275 km: T_P (200)=1231 °C, T_P (225)=1281 °C, T_P (250)=1311 °C, and T_P (275)=1317 °C. 1200 and 1300 °C adiabats with a gradient of 0.4 °C/km are shown by a dashed curve.

correlation between P- and S-velocities [56] leads to the discrepancies reaching 300–500 °C, which may be attributed mainly to not correctly modeled S-velocities with a fixed Poisson ratio of 0.27.

The second is the offset of T_P and T_S with opposite signs at depths below 210 km. Fig. 5 illustrates an offset of T_P(PM) to higher temperatures compared to GP composition because the PM model has higher P-velocity (but not S-velocity, Fig. 2) and density than the GP composition at fixed P–T conditions. In contrast to T_P, Fig. 5 shows an offset of T_S(PM) to lower temperatures compared to T_S(GP). This means that compositional effects are present in both seismic models. This means also that a sharp change in composition from depleted to fertile mantle, leading to an offset of T_P and T_S with opposite signs, cannot explain the temperature anomalies at depths below 210 km and may lead to misinterpretations of the upper mantle composition. A mantle either with a uniform composition or with a jump in composition would reveal decreasing T_P and T_S with depth. Negative temperature gradients and opposite

signs in T_P and T_S provide strong evidence that a gradual change in chemistry occurs at depths below ~210 km.

For the average continental mantle, we speculate that these temperature anomalies can be easily explained by the compositional heterogeneity of the upper mantle. This implies that upper mantle compositions may reflect variable extent of fertility with depth. However, a more detailed seismological study is needed to test this interpretation. At the same time, it would not be unreasonable to assume that temperature anomalies for the normal mantle can be associated with a high-gradient zone in the IASP91 model at depths of 210–300 km.

Figs. 3–5 show that a uniform composition or a sharp change in composition from depleted garnet peridotite to fertile pyrolitic material seems unable to explain the enigmatic inflexions of geotherms as well as an anticorrelated behavior for T_P and T_S inferred from P- and S-velocities. Because compositional effects play a dominant role in determining the temperatures from regional seismic models, we arrive to a conclusion about the impossibility of a uniform composition throughout the entire Kaapvaal cratonic mantle. This may suggest a strong compositional gradient below ~200 km and a vertical zonation in the composition of the Kaapvaal lithospheric mantle. According to [51], a lithospheric mantle would be expected to be chemically stratified, becoming more fertile in composition with depth.

The seismic velocities are continuous across 220 km depth [58]. The observed increasing velocity profiles in the Kaapvaal cratonic mantle [56,57,60] must be controlled by consistent changes in the mantle bulk composition and mineralogy with depth. The only reasonable way to eliminate kinks on geotherms and to get monotonous temperature profile is by changing the bulk composition with depth. Fig. 5 shows the T_P estimates from the BPI1A P-velocity model obtained when P-velocities are inverted assuming variable bulk composition. The change in composition with depth is determined by trial and error.

As the starting point, we have used the fixed bulk composition of the average garnet peridotite (GP model from Table 1) at depths between 100 and 175 km; Mg# 92.0. At depths between 200 and 275 km, a change in composition in terms of the major element contents and an increase in fertility (gradual increase in FeO (from 7 to 8 wt.%), Al_2O_3 (from 1.3 to 4.5 wt.%), and CaO (from 0.8 to 3.5 wt.%)) are performed; a decrease in MgO content is from 45.3 to 38.6 wt.%. Define this variable composition as GP*, which is approaching to the PM composition [51,77] at 275 km depth (Table 3). Phase proportions (mol%) are changing from 65.6% Ol ($Fo_{92.5}$)+1.4% Gar+27% Opx+6% Cpx at 100–175 km (Table 1) to 59.7% Ol ($Fo_{91.9}$)+5.7% Gar+34.5% Cpx (± Ilm) at 275 km and 1317 °C. Orthopyroxene content decreases whereas garnet content increases with depth. At the deeper mantle, the increase in fertility is accompanied by a change in phase proportions and a decrease in Mg# from 92.0 to 89.6 (275 km). Fo^{oliv} decreases with increasing depth in agreement with petrologic data [78]. The change in phase proportions is accompanied by a significant increase in mantle density: ρ(175 km/1138 °C)=3.34 g cm^{-3} and ρ(275 km/1317 °C)=3.465 g cm^{-3} (Table 3).

Table 3
Velocity and density models for southern Africa

H (km)	$T_{P,S}$ (°C)	V_P (BPI1A) [57] (km s^{-1})	V_S (V_S–BPI1A) (km s^{-1})	ρ (GP*)[a] (g cm^{-3})
100	1049	8.131	4.544	3.279
125	1077	8.204	4.566	3.300
150	1049	8.298	4.612	3.327
175	1138	8.331	4.602	3.339
200	1231	8.370	4.584	3.361
225	1281	8.427	4.586	3.396
250	1311	8.498	4.608	3.429
275	1317	8.583	4.643	3.465

[a]The average garnet peridotite (GP model from Table 1) is used at depths between 100 and 175 km. An increase in fertility is assumed at greater depths; TiO_2=0.08% at all depths. Variations of the GP* composition are as follows (in wt.%). At 200 km depth — SiO_2=44.97%, MgO=44.3%, FeO=7.3%, CaO=1.4%, Al_2O_3=1.8%, Na_2O=0.15%; at 250 km — SiO_2=44.97%, MgO=40.5%, FeO=7.9%, CaO=2.8%, Al_2O_3=3.5%, Na_2O=0.25%; at 275 km — SiO_2=45.00%, MgO=38.6%, FeO=8.0%, CaO=3.5%, Al_2O_3=4.5%, Na_2O=0.32%.

The variations in bulk and modal composition with depth result in the disappearance of the non-physical inflection of the temperature profile derived from the BPI1A model at depths between 200 and 275 km (Fig. 5). A comparison of geotherms (Figs. 3, 4 and 5) shows that an erroneous estimate of the cratonic composition has the considerable effect on the position of the calculated geotherms. Thus, to avoid temperature inflexions, gradual changes in composition and mantle mineralogy with depth are required to get a monotonous temperature profile. However, the detailed study of the compositional structure of the cratonic upper mantle is well beyond the scope of this work.

Regional P and S models (often not well constrained) yield incompatible velocities for the lithospheric mantle under the Kaapvaal craton [56,57,60,62]. Poor correlation between P- and S-velocity models [56] leads to incompatible temperature estimates derived from the two velocity models with the discrepancies in T_P and T_S reaching 300–500 °C at depths below 200 km (Fig. 5). Disagreement between T_P and T_S (Figs. 3 and 5) can be attributed to seismic anomalies, and differences in

absolute velocities and velocity gradients in regional models (Fig. 1).

Discussion of evidence for a low-velocity zone in the mantle beneath the Kaapvaal craton is controversial [55–65]. The LVZ is not detected for P-waves in model BPI1A [57], but the LVZ is found for S-waves within the Kaapvaal craton in model BPISM [64]. To find out internal consistency between the two models, absolute S-velocities (defined here as model V_S_BPI1A) are computed from the BPI1A P-velocity model for the upper mantle below and around the Kaapvaal craton [57]. To calculate S-velocity model consistent with P-velocities from BPI1A, we use the same GP* composition and temperatures, inferred from BPI1A, as well as anharmonic and anelastic parameters. For example, if we have the P-velocity value of 8.427 km s^{-1} at 225 km depth [57], the inferred temperature ($T_P = T_S$) and S-velocity will be 1281 °C and 4.586 km s^{-1} (V_S(Anh) = 4.624 km s^{-1}) if the composition is GP*. The behavior of shear velocity model V_S_BPI1A in comparison with the IASP91 model and model V_P_Poisson is shown in Fig. 6 and Table 3.

In contrast to model V_P_Poisson [56], model V_S _ BPI1A reveals that a weakly expressed LVZ is present at depths between 150 km and 250 km (Fig. 6). The velocity structure of the V_S_BPI1A model confirms that it is possible to have a LVZ for shear waves as was found in model BPISM without requiring one for compressional waves [64]. This conclusion is not in contradiction with that reported in [58] whose results show no evidence for a substantial LVZ for S-waves within the Kaapvaal craton.

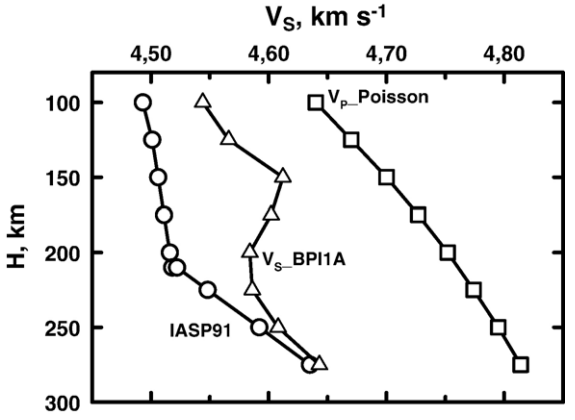

Fig. 6. S-velocity model V_S_BPI1A derived from the BPI1A P-velocity profile [57] for the GP* composition. T_S inferred from model V_S_BPI1A are identical to T_P inferred from model BPI1A (Fig. 5, Table 3). Model V_S_BPI1A reveals a solid-state low-velocity zone, while model V_P_Poisson has no LVZ. At depths below 250 km, model V_S_BPI1A for cratonic mantle and the IASP91 model converge.

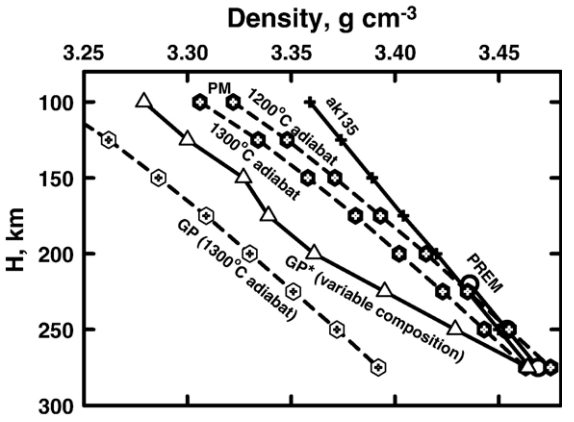

Fig. 7. Density profiles. The calculated densities for cratonic mantle with a variable GP* composition and for primitive mantle composition are compared to the PREM and *ak*135 model density. The density of the GP and PM models from Table 1 has been calculated using an adiabat of 0.4 °C km^{-1}. At 275 km depth (~9 GPa), the density of the GP* and PM compositions as well as the PREM and *ak*135 model density converge; ρ(GP*/275 km and 1317 °C) = 3.465 g cm^{-3} (Table 3) is close to ρ(PM) between 1200 and 1300 °C adiabats (ρ(275 km/1310 °C) = 3.475 g cm^{-3} and ρ(275 km/1410 °C) = 3.463 g cm^{-3}).

The solid state LVZ with a GP* composition, satisfying seismic model BPI1A and petrological requirements (mantle xenoliths) and located within the cratonic lithosphere, does not suggest the existence of hydrous phases and partial melt-bearing asthenosphere.

Model BPISM is characterized by a LVZ at depths between 210 and 350 km with a wavespeed ranging from 4.52 km s^{-1} (however, this value is identical to that of IASP91 for the normal mantle at 210 km depth) to 4.70 km s^{-1} [64], while model V_S_BPI1A has a "cold" low-velocity zone at depths of 150 and 250 km with V_S between 4.58 and 4.61 km s^{-1} (Fig. 6, Table 3). At 210-km depth our S-wave velocity model is increased from BPISM (and from IASP91) by 0.065 km s^{-1} (~1.5% in V_S of BPISM). As was noted above, a temperature inflection with a negative temperature gradient at depths between 125 and 150 km (Fig. 4, Table 3) might be attributed to a high BPI1A velocity gradient at these depths. Our V_S estimates are consistent with the cratonic velocity value of 4.61 km s^{-1} at 220 km from surface-wave data [58] and with the IASP91 model at 275 km. This assumes that a GP* model is approaching to primitive mantle composition at depths below 250 km (Tables 1 and 3), where S-velocity and density profiles for cratonic mantle and seismic models converge (Figs. 6 and 7).

The calculated densities for the GP* composition for cratonic mantle and for primitive mantle composition

are compared to the PREM and *ak*135 model density [79,80] (Fig. 7). Recall that GP* composition is derived from model BPI1A in order that to avoid temperature inflexions. Seismic models are non-unique. Consequently, this composition is non-unique and should be considered only as an example of the possible change in mineralogy from highly depleted to fertile material. In general, compositional spectrum of cratonic peridotites and lithospheric thickness can vary from craton to craton, depending on their stabilization age, tectonic history and geothermal regime [29,81]. The GP* cratonic lithosphere is less dense than *ak*135 at shallow depths, but below 250 km depth the GP* density gradually increases approaching to the primitive mantle density as well as to the PREM and *ak*135 models. Assuming primitive mantle composition, the density of the normal mantle at 275 km is estimated to be between 3.475 and 3.463 g cm^{-3} for 1200 and 1300 °C adiabats (Fig. 7).

Our results show that chemically depleted lithosphere beneath the Kaapvaal craton exists to depths of about 175–200 km. At greater depths (~200–250 km), the lithospheric material appears to be substantially enriched in FeO and refractories (Al_2O_3 and CaO) compared to the depleted GP compositions (i.e., low-*T* and high-*T* xenoliths) but simultaneously also must be more depleted than primitive mantle. Thus, the mantle composition in a depth range of 200 and 250 km is more enriched than the overlying mantle but it is more depleted than underlying fertile mantle. At depths of about 275 km, Kaapvaal cratonic mantle does not differ from normal mantle (Figs. 6 and 7). This more fertile and denser mantle sublayer, which is cooler than average upper mantle at the same depth (Fig. 5), is similar but not identical to the results of Lee et al. [82]. Such layered structure suggests that a transition sublayer in the depth range of 200–275 km may be a more complex feature than previously thought and models to explain it should take into account significant variations in chemical composition and phase proportions of coexisting phases.

We thus derive a lithosphere thickness of roughly 275 km for the Kaapvaal craton. The location of the base of the lithosphere can be approximated by the intersection of temperature derived from model BPI1A and mantle adiabat (Fig. 5). This assumption is confirmed by the intersection of S-velocity and density profiles for the GP* composition with those from seismic models at a depth of 275 km (Figs. 6 and 7). The analysis presented above suggests that the cold ancient Kaapvaal craton has no partial melt-bearing asthenosphere and the thickness of its lithospheric root reaches ~275 km, which is consistent with P-wave and S-wave tomographic images of upper mantle structure beneath southern Africa [22,55]. We find no evidence that the Lehmann discontinuity exists beneath the Kaapvaal mantle. This is consistent with the results of Gao et al. [61].

The basic conclusion arising from this study is that the results admit continuous variations in bulk chemistry and a substantial increase in fertility at depths below 200 km, and assume that the mantle beneath the Kaapvaal craton is chemically stratified. Note that a similar layered structure, i.e., refractory assemblages underlain by fertile lithologies, has been proposed for some Archean cratons within the Slave, Siberian, Tanzanian and Sarfatoq lithospheres [41,78,83,84]. At the base of the lithosphere (~275 km) of the Kaapvaal craton, the chemical composition of the mantle keel contains abundances of major elements, which are generally similar to the estimates of primitive mantle composition [51,77].

4. Uncertainty estimates

Interpretation of the temperature distribution in the mantle is associated with a number of uncertainties, including errors in the calculated bulk properties of the phase assemblages existing under high pressures and temperatures, and our limited knowledge of the current thermal state and compositional heterogeneity of the Earth's interior. In this section, we consider briefly some of these effects.

4.1. Uncertainties in thermodynamic parameters

Thermodynamic (elastic) and anelastic properties of minerals and temperature and pressure effects are the most important parameters controlling density and seismic velocities of a multiphase mantle material. Comprehensive quantification of the uncertainties is difficult because of the complex and multivariant nature of the problem [12–14,85]. However, applying suitable models for the equation of state of minerals and solid solutions and self-consistent thermodynamic properties of mineral end-members, phase diagrams and bulk properties of the mantle composite can be evaluated with confidence [26–28]. For a given chemical composition (Table A), the effect of temperature variations of ±100 °C causes less than ±0.015 g cm^{-3} (±0.4%) density variations and ±0.04 km s^{-1} (±0.5% for V_p and ±0.8% for V_s) P- and S-velocity variations, that is close to estimated uncertainties in P-velocities [85]. Discrepancies and contradictions among available seismic models for Kaapvaal craton are significantly

Table 4
Thermochemical and thermoelastic properties of minerals at 1 bar 298.15 K

Properties	$MgSiO_3$ orthoenstatite	Cr_2O_3 eskolaite	Mg_2SiO_4 forsterite	$MgCr_2O_4$ spinel	$Mg_3Cr_2Si_3O_{12}$ knorringite
V (cm^3 mol^{-1})	31.37	29.05	43.67	43.56	117.475
α (10^6, K^{-1})	28.6	18.6	27.1	16.5	22.2
K_S (kbar)	1077	2320	1288	2000	1730
dK_S/dP	5.0	4.0	4.2	5	4.5
Θ (K)	731	775	762	760	760
γ	1.03	1.24	1.28	1.12	1.28
G (kbar)	760	1300	810	1100	920
dG/dP	1.6	1.8	1.4	0.5	1.6
dG/dT (kbar K^{-1})	−0.11	−0.19	−0.13	−0.1	−0.10
V_P (km s^{-1})	8.08	8.80	8.57	8.86	8.76
V_S (km s^{-1})	4.87	4.98	5.01	4.99	4.88
$\Delta_f H^o_{298}$ (kJ mol^{-1})	−1546.24	−1128.2	−2174.14	−1762.0	−5692.2 [a] −5676.7 [b] −5542.0 [c]
S^o_{298} (J $mol^{-1}\cdot K^{-1}$)	66.25	83.1	94.1	119.6	304.6[a] 318.9[b] 377.0[c]

Comment to Table 4.
$MgSiO_3$, Mg_2SiO_4 — enthalpy ($\Delta_f H^o_{298}$), entropy (S^o_{298}), heat capacity (C_p, J mol^{-1} K^{-1}), Grüneisen parameter ($\gamma = V\cdot K_S\cdot\alpha/C_p$), thermal expansion and bulk moduli for orthoenstatite and forsterite from Ref. [69]; C_p ($MgSiO_3$) = $178.1 - 0.015T - 298450.00T^{-2} - 1592.65T^{-1/2}$.
$C_p(Mg_2SiO_4) = 234.9 + 0.001069T - 542900.0T^{-2} - 1906.4T^{-1/2}$.
Cr_2O_3 — enthalpy, entropy and $C_p = 227.25 - 0.02132T + 3543029T^{-2} - 2567.3T^{-1/2}$ [88]; V, K_S, G, α [90]; dK_s/dP, dG/dP, dG/dT are taken as for Al_2O_3 [69]; γ, Θ, V_P and V_S — this study.
$MgCr_2O_4$ — enthalpy, entropy, V and $C_p = 221.24 - 0.0010203T - 1757210T^{-2} - 1247.9T^{-1/2}$ [88]; α [90]; K_S, G, dK_s/dP, dG/dP, dG/dT are taken as for $MgAl_2O_4$ [69]; γ, Θ, V_P and V_S — this study.
$Mg_3Cr_2Si_3O_{12}$ — V, α, $C_p = 506.61 + 0.029457T - 1298.40T^{-1/2} - 7876200.0T^{-2}$ [86,89]; K_S, G, dK_S/dP, dG/dP, dG/dT are the same as for pyrope [69]; γ, Θ, V_P and V_S — this study.
[a] $\Delta_f H^o_{298}$ and S^o_{298} are estimated from P–T data of Doroshev et al. [86] for reaction (I).
[b] $\Delta_f H^o$ and S^o_{298} are estimated from P–T data of Klemme [87] for reaction (II).
[c] $\Delta_f H^o_{298}$ and S^o_{298} are estimated by Klemme [87].

larger. Uncertainties in the model and EOS parameters can affect calculated absolute velocities and temperatures but cannot affect the presence or absence of inflexions in temperature profiles, because T_P and T_S were calculated in simultaneous inversion from the same seismic models and the effect of uncertainties on T_P and T_S should be similar.

4.2. Effect of Cr

We have ruled out such an important element for the composition of garnet peridotites as chromium as less significant for the seismic properties of the deep interior and because of lack of necessary thermochemical and thermoelastic data for such the end-members $Ca_3Cr_2Si_3O_{12}$, $Fe_3Cr_2Si_3O_{12}$ and $Mg_3Cr_2Si_3O_{12}$ (knorringite, Kn). Rigorous thermodynamic modeling of phase transitions and physical properties in the mantle requires reliable thermodynamic data for Cr-bearing garnets. Thermodynamic properties of knorringite garnet have been estimated from high-pressure–high-temperature experimental data according to the reactions (I) and (II), [86,87] and EOS of minerals [69,88–90] (Table 4). Reaction (I) was studied in the range of 8–9.5 GPa and 1000–1800 °C [86] and reaction (II) was studied in the range of 4.5–16 GPa and 1200–1600 °C [87]:

$$Mg_3Cr_2Si_3O_{12}(Kn) = 3MgSiO_3(orthoenstatite) + Cr_2O_3(eskolaite), \quad (I)$$

$$MgCr_2O_4(spinel) + 4MgSiO_3(orthoenstatite) = Mg_3Cr_2Si_3O_{12}(Kn) + Mg_2SiO_4(forsterite) \quad (II)$$

Thermodynamic evaluation of the experimental data yields for knorringite (Table 4): $\Delta_f H^o_{298} = -5692.2$ kJ mol^{-1} and $S^o_{298} = 304.6$ J mol^{-1} K^{-1} from reaction (I); $\Delta_f H^o_{298} = -5676.7 \pm 6.0$ kJ mol^{-1} and $S^o_{298} = 318.9 \pm 2.0$ J mol^{-1} K^{-1} from reaction (II). The calculated values of $\Delta_f H^o_{298}$ and S^o_{298} for knorringite from both reactions are in reasonable agreement with each other and with estimates [91] but are in strong disagreement with estimates of Klemme [87]: $\Delta_f H^o_{298} = -5542$ kJ mol^{-1} and $S^o_{298} = 377$ J mol^{-1} K^{-1}. The calculated values of S^o_{298} are close to estimated value of S^o_{298} (Kn) ≈ 325 J mol^{-1} K^{-1} [91] and

to the exchange entropy S^{o}_{298} (Kn) $\approx S^{o}$ (pyrope) $+ S^{o}$ ($MgCr_2O_4$) $- S^{o}$ ($MgAl_2O_4$) $= 266.3 + 119.6 - 82.82 = 303.1$ J mol^{-1} K^{-1}. Thermodynamic parameters of knorringite from Table 4 were used to estimate the effect of Cr on physical properties of the ideal pyrope–knorringite solid solution. Calculations show that for Cr-bearing garnet containing 10 mol% of knorringite, P- and S-velocities decrease by 0.4% while density increases by 0.8% compared to pure pyrope. For the bulk mantle composition with 0.4 wt.% of Cr_2O_3 [51], the influence of Cr on physical properties of Cr-bearing assemblages shows only negligible effects on velocities and densities.

4.3. Effect of anisotropy

Isotropic velocities have been assumed in the present study. Our results may therefore be biased by the presence of anisotropy. Seismic properties of six upper mantle xenoliths from South Africa, varied from mica peridotite to garnet harzburgite, were determined by ultrasonic measurements at elevated pressure and by numerical calculations from petrofabric analyses [92]. Measured and calculated average anisotropies are about 5% for V_P and 4% for V_S. By interpolating to in situ P–T conditions (4 GPa (~125 km), 950°C), Long and Christensen [92] obtained V_P of 8.31 km s^{-1} and V_S of 4.75 km s^{-1}. At these P–T conditions their P-velocity is in excellent agreement with the fastest model of Zhao et al. [56] (8.32 km s^{-1} at 125 km depth) and our isotropic velocity value for the GP composition ($V_P = 8.28$ km s^{-1}) but is significantly higher than that of Qiu et al. [62] and Simon et al. [57]. However, their S-velocity at 125 km depth is significantly higher than that in the VF model [60] (4.52 km s^{-1}) and in model V_p–Poisson [56] (4.67 km s^{-1}), and than the calculated value for the GP composition ($V_S = 4.64$ km s^{-1}). Our calculations show (Fig. 1) that isotropic velocities calculated for the GP model are between the fastest and slowest seismic models for the Kaapvaal craton. According to [58], anisotropy terminates at a depth of 100 km beneath the Kaapvaal. As the in situ orientation of xenoliths is generally unknown, it is difficult to reconcile laboratory and seismic data (see for further discussion [58,59,61, 93,94]). In any case, anisotropy cannot explain inflected profiles at depths below 200 km. Thus, we may conclude that contribution from anisotropy is unlikely to be of a major effect on our results.

5. Summary and conclusion

In this study we infer the temperature distribution models for the mantle beneath the Kaapvaal craton from absolute P- and S-wave velocities and geochemical constraints on garnet peridotite and primitive mantle compositions. Unlike the previous studies, we used a self-consistent thermodynamic approach, which requires a small number of thermodynamically defined parameters and has important advantages over procedures, which contain no information about entropy, enthalpy and Grüneisen parameter. This approach yields the self-consistent information on multiphase mineral assemblages (phase proportions and chemical composition of coexisting phases), density and velocities and provides the more reliable constraints on the thermal and compositional structure of the cratonic mantle from combining seismic models with mineral physics data. The results permit the following conclusions.

(1) Distributions of density and P- and S-wave velocities for the Kaapvaal cratonic mantle in the depth range of 100–300 km depth and at 800–1600 °C are calculated for low-T and high-T garnet peridotite xenoliths, average depleted garnet peridotite (GP) and primitive mantle composition (PM). Calculated velocities are between the fastest and slowest seismic models reported for southern Africa. Sensitivity of density and seismic velocities to temperature, pressure and composition was numerically studied. At the same P–T conditions, the PM composition has significantly higher density than the GP composition ($\Delta\rho/\rho \approx 2\%$) but similar velocities: P-velocities for the PM are higher by ~0.4% than for the GP, whereas S-velocities for the PM are lower by 0.4–0.6% than for the GP. Thermodynamic properties of knorringite garnet and the influence of Cr on physical properties of Cr-bearing garnets have been estimated.

(2) Poor correlation between the regional P- and S-wave velocities under the Kaapvaal craton leads to temperature discrepancies reaching 300–500 °C. Despite the geotherms inferred from seismic observations under the Kaapvaal craton show an appreciable scatter, cratonic mantle is significantly cooler than average upper mantle at least to 200–250 km depths. Temperatures inferred from P- and S-velocities of the IASP91 model agree reasonably well with each other and are significantly higher than those from the regional models. However, the IASP91 P- and S-velocity profiles with maximal T_P and T_S at 210 km lead to a temperature inflection with a negative temperature gradient at depths below 210 km, resulting in non-physical temperature behavior. For the average

continental mantle, we assume that temperature anomalies can be explained either by the compositional heterogeneity of the upper mantle or by seismic uncertainties associated with the high velocity gradients in the IASP91 model at depths of 210–300 km. Except for the fastest models [56], temperatures inferred from the regional BPI1A, QPM and VF models display an inflection both for depleted and fertile compositions at depths between about 220 and 250 km. Because P- and S-velocities of all considered models increase monotonically with depth, it is impossible to explain the kinks of geotherms by the presence of partial melt, hydrous phases or volatiles, all of which must lower mantle velocities, or by phase transitions.

(3) Despite composition-induced velocity variations are significantly less than seismic discrepancies at depths of 100–250 km, composition remains the most important factor in controlling mantle temperatures derived from velocity models for southern Africa. Temperatures depend rather strongly on bulk composition and proportion of phases stable at various depths of the upper mantle. The relatively small differences between the xenolith compositions translate into appreciable variations in inferred temperature. The results of our inversion procedure indicate that upper mantle compositions at depths above and below ~200 km are strikingly different. The mantle beneath the Kaapvaal craton cannot be treated as uniform in terms of chemical composition because a fixed uniform composition leads to a non-physical behavior of the geotherms. Either low-T and high-T peridotites, depleted in Fe, Al and Ca, or fertile asthenospheric material (PM model), enriched in Fe, Al and Ca, cannot explain the nature of the inflections below 200 km. A sharp change in composition from depleted garnet peridotite to fertile pyrolitic material seems unable to explain inflexions of geotherms as well as an anticorrelated behavior for T_P and T_S inferred from P- and S-velocities. To avoid temperature inflexions, continuous variations in bulk chemistry and a substantial increase in fertility (gradual increase in FeO, Al_2O_3 and CaO content) at depths between 200 and 275 km are required to get monotonous temperature profiles. At depths of about 275 km, Kaapvaal cratonic mantle does not differ from normal mantle. Our results assume that the mantle beneath the Kaapvaal craton is chemically stratified: an upper layer at depths between 100 and 175 km consists of depleted garnet peridotite and a lower layer (200–275 km), which is characterized by a more fertile material, enriched in FeO and refractories.

(4) S-velocity and density model for southern Africa is constructed. The results indicate the possibility of the existence of a solid-state low-velocity zone at depths between 150 km and 250 km, which may be associated with temperature gradients alone without hydrous phases and partial melting. The thickness of the Kaapvaal lithospheric root reaches ~275 km, which is consistent with P-wave and S-wave tomographic images of upper mantle structure beneath southern Africa [22,55].

Acknowledgements

This research was supported by the Royal Swedish Academy of Sciences and by Russian Academy of Sciences under Programs 25 and 27, and by RFBR grants (03-05-64412 and 06-05-64151). O.L.K. enjoyed the hospitality of Department of Earth Sciences of Uppsala University. We are grateful to I. Artemieva, A. Girnis, L. Vinnik, and A. Ukhanov for their useful comments and numerous discussions, and S.King and anonymous reviewers for reviews and editorial suggestions. Detailed comments of the manuscript by I. Artemieva led to a number of improvements in the final draft and her comments are greatly appreciated.

Appendix A

Table A
Calculated density, P- and S-velocities for depleted garnet peridotite (GP) and primitive mantle (PM) with bulk compositions from Table 1

H (km)	P (GPa)	T (°C)	V_p (km s^{-1})	V_s (km s^{-1})	ρ (g cm^{-3})
Garnet peridotite					
100	3.1	800	8.262	4.663	3.314
100	3.1	1000	8.181	4.594	3.287
125	3.95	900	8.297	4.656	3.324
125	3.95	1100	8.220	4.588	3.297
150	4.8	1000	8.331	4.649	3.333
150	4.8	1200	8.256	4.582	3.307
175	5.6	1100	8.364	4.642	3.343
175	5.6	1300	8.291	4.575	3.317
200	6.45	1200	8.398	4.635	3.352
200	6.45	1400	8.325	4.568	3.327
250	8.15	1300	8.498	4.654	3.383
250	8.15	1500	8.429	4.589	3.358
Primitive mantle					
100	3.1	800	8.270	4.629	3.383
100	3.1	1000	8.188	4.559	3.357

(continued on next page)

Table A (*continued*)

H (km)	P (GPa)	T (°C)	V_p (km s^{-1})	V_s (km s^{-1})	ρ (g cm^{-3})
125	3.95	900	8.310	4.625	3.394
125	3.95	1100	8.231	4.557	3.368
150	4.8	1000	8.348	4.621	3.405
150	4.8	1200	8.271	4.554	3.379
175	5.6	1100	8.382	4.616	3.414
175	5.6	1300	8.308	4.550	3.389
200	6.45	1200	8.418	4.613	3.423
200	6.45	1400	8.346	4.547	3.399
250	8.15	1300	8.522	4.637	3.454
250	8.15	1500	8.453	4.573	3.430
300	9.85	1500	8.590	4.631	3.472
300	9.85	1600	8.557	4.599	3.461

References

[1] I.M. Artemieva, W.D. Mooney, Thermal thickness and evolution of Precambrian lithosphere: a global study, J. Geophys. Res. 106 (2001) 16387–16414.

[2] G. Nolet, S.P. Grand, B.L.N. Kennett, Seismic heterogeneity in the upper mantle, J. Geophys. Res. 99B (1994) 23753–23766.

[3] H.N. Pollack, S.J. Hurter, J.R. Johnson, Heat flow from the Earth's interior: analysis of the global data set, Rev. Geophys. 31 (1993) 267–280.

[4] R.L. Rudnick, W.F. McDonough, R.J. O'Connell, Thermal structure, thickness and composition of continental lithosphere, Chem. Geol. 145 (1998) 395–411.

[5] C. Jaupart, J.C. Mareschal, The thermal structure and thickness of continental roots, Lithos 48 (1999) 93–114.

[6] A.H.E. Röhm, R. Snieder, S. Goes, J. Trampert, Thermal structure of continental upper mantle inferred from S-wave velocity and surface heat flow, Earth Planet. Sci. Lett. 181 (2000) 395–407.

[7] F. Deschamps, J. Trampert, R. Snieder, Anomalies of temperature and iron in the uppermost mantle inferred from gravity data and tomographic models, Phys. Earth Planet. Inter. 129 (2002) 245–264.

[8] F. Cammarano, S. Goes, P. Vacher, D. Giardini, Inferring upper-mantle temperatures from seismic velocities, Phys. Earth Planet. Inter. 138 (2003) 197–222.

[9] T.H. Jordan, Mineralogies, densities and seismic velocities of garnet lherzolites and their geophysical implications, in: F.R. Boyd, H.O.A. Meyer (Eds.), The Mantle Sample: Inclusions in Kimberlites and Other Volcanics, AGU, Washington, DC, 1979, pp. 1–14.

[10] V.A. Kronrod, O.L. Kuskov, Determination of temperature and bulk composition of the upper mantle from seismic data, Geochem. Int. 34 (1996) 72–76.

[11] F. Cammarano, S. Goes, A. Deuss, D. Giardini, Is a pyrolitic adiabatic mantle compatible with seismic data? Earth Planet. Sci. Lett. 232 (2005) 227–243.

[12] C.-T.A. Lee, Compositional variation of density and seismic velocities in natural peridotites at STP conditions: implications for seismic imaging of compositional heterogeneities in the upper mantle, J. Geophys. Res. 108 (B9) (2003) 2441, doi:10.1029/2003JB002413.

[13] N.M. Shapiro, M.H. Ritzwoller, Thermodynamic constraints on seismic inversions, Geophys. J. Int. 157 (2004) 1175–1188.

[14] S.V. Sobolev, H. Zeyen, G. Stoll, F. Werling, R. Altherr, K. Fuchs, Upper mantle temperatures from teleseismic tomography of French Massif Central including effects of composition, mineral reactions, anharmonicity, anelasticity and partial melt, Earth Planet. Sci. Lett. 139 (1996) 147–163.

[15] S.V. Sobolev, H. Zeyen, H. Granet, U. Achauer, C. Bauer, F. Werling, R. Altherr, K. Fuchs, Upper mantle temperatures and lithosphere–asthenosphere system beneath the French Massif Central constrained by seismic, gravity, petrologic and thermal observations, Tectonophysics 275 (1997) 143–164.

[16] S. Goes, R. Govers, P. Vacher, Shallow mantle temperatures under Europe from P and S wave tomography, J. Geophys. Res. 105B (2000) 11153–11169.

[17] S. Goes, S. van der Lee, Thermal structure of the North American uppermost mantle inferred from seismic tomography, J. Geophys. Res. 107B (2002), doi:10.1029/2000JB000049.

[18] S. Goes, F.J. Simons, K. Yoshizawa, Seismic constraints on temperature of the Australian uppermost mantle, Earth Planet. Sci. Lett. 236 (2005) 227–237.

[19] K. Kuge, Y. Fukao, High-velocity lid of East Antarctica: evidence of a depleted continental lithosphere, J. Geophys. Res. 110B (2005) B06309, doi:10.1029/2004JB003382.

[20] I.M. Artemieva, M. Billien, J.-J. Lévêque, W.D. Mooney, Shear wave velocity, seismic attenuation, and thermal structure of the continental upper mantle, Geophys. J. Int. 157 (2004) 607–628, doi:10.1111/j.1365-246X.2004.02195.x.

[21] T.H. Jordan, Composition and development of the continental tectosphere, Nature 274 (1978) 544–548.

[22] D.E. James, F.R. Boyd, D. Schutt, D.R. Bell, R.W. Carlson, Xenolith constraints on seismic velocities in the upper mantle beneath southern Africa, Geochem. Geophys. Geosyst. 5 (2004), doi:10.1029/2003GC000551.

[23] Y.H. Poudjom Djomani, S.Y. O'Reilly, W.L. Griffin, P. Morgan, The density structure of subcontinental lithosphere through time, Earth Planet. Sci. Lett. 184 (2001) 605–621.

[24] M.K. Kaban, P. Schwintzer, I.M. Artemieva, W.D. Mooney, Density of the continental roots: compositional and thermal contributions, Earth Planet. Sci. Lett. 209 (2003) 53–69.

[25] R. Jeanloz, A.B. Thompson, Phase transitions and mantle discontinuities, Rev. Geophys. Space Phys. 21 (1983) 51–74.

[26] O.L. Kuskov, A.B. Panferov, Phase diagrams of the FeO–MgO–SiO_2 system and the structure of the mantle discontinuities, Phys. Chem. Miner. 17 (1991) 642–653.

[27] O.B. Fabrichnaya, O.L. Kuskov, Constitution of the mantle. 1. Phase relations in the FeO–MgO–SiO_2 system at 10–30 GPa, Phys. Earth Planet. Inter. 69 (1991) 56–71.

[28] O.L. Kuskov, O.B. Fabrichnaya, L.M. Truskinovsky, Constitution of the mantle. 2. Petrological models of transition zone based on FMS phase diagram, Phys. Earth Planet. Inter. 69 (1991) 72–84.

[29] S.D. King, Archean cratons and mantle dynamics, Earth Planet. Sci. Lett. 234 (2005) 1–14.

[30] B.J. Wood, J.R. Holloway, Theoretical prediction of phase relationships in planetary mantles, J. Geophys. Res., Suppl. 87 (1982) A19–A30.

[31] S.K. Saxena, G. Eriksson, Theoretical computation of mineral assemblages in pyrolite and lherzolite, J. Petrol. 24 (1984) 538–555.

[32] O.L. Kuskov, R.F. Galimzyanov, Thermodynamics of stable mineral assemblages of the mantle transition zone, in: S.K. Saxena (Ed.), Chemistry and Physics of the Terrestrial Planets, Springer, New York, 1986, pp. 310–361.

[33] O.B. Fabrichnaya, O.L. Kuskov, Constitution of the Moon: 1. Phase relations in the FeO–MgO–Al_2O_3–SiO_2 system, Phys. Earth Planet. Inter. 83 (1994) 175–197.
[34] J. Ita, L. Stixrude, Petrology, elasticity and composition of the mantle transition zone, J. Geophys. Res. 97 (1992) 6849–6866.
[35] S.K. Saxena, Earth mineralogical model: Gibbs free energy minimization computation in the system MgO–FeO–SiO_2, Geochim. Cosmochim. Acta 60 (1996) 2379–2395.
[36] O.L. Kuskov, Constitution of the Moon: 3. Composition of middle mantle from seismic data, Phys. Earth Planet. Inter. 90 (1995) 55–74.
[37] O.L. Kuskov, Constitution of the Moon: 4. Composition of the mantle from seismic data, Phys. Earth Planet. Inter. 97 (1997) 239–257.
[38] L. Stixrude, C. Lithgow-Bertelloni, Mineralogy and elasticity of the oceanic upper mantle: origin of the low-velocity zone, J. Geophys. Res. 110(B3) (2005) B03204, doi:10.1029/2004JB002965.
[39] O.L. Kuskov, V.A. Kronrod, Constitution of the Moon: 5. Constraints on composition, density, temperature, and radius of a core, Phys. Earth Planet. Inter. 107 (1998) 285–306.
[40] B.L.N. Kennet, E.R. Engdahl, Travel times for global earthquake location and phase identification, Geophys. J. Int. 105 (1991) 429–465.
[41] M.G. Kopylova, J. Lo, N.I. Christensen, Petrological constraints on seismic properties of the Slave upper mantle (northern Canada), Lithos 77 (2004) 493–510.
[42] C. de Capitani, T.H. Brown, The computation of equilibrium in complex systems containing non-ideal solutions, Geochim. Cosmochim. Acta 51 (1987) 2639–2652.
[43] L. Thomsen, Theoretical foundations of equations of state for the terrestrial planets, Ann. Rev. Earth Planet. Sci. 5 (1977) 491–513.
[44] S. Karato, Importance of anelasticity in the interpretation of seismic tomography, Geophys. Res. Lett. 20 (1993) 1623–1626.
[45] I. Jackson, S.M. Rigden, Composition and temperature of the Earth's mantle: seismological models interpreted through experimental studies of Earth materials, in: I. Jackson (Ed.), The Earth's Mantle: Composition, Structure, and Evolution, Cambridge Univ. Press, Cambridge, 2000, pp. 405–460.
[46] U.H. Faul, I. Jackson, The seismological signature of temperature and grain size variations in the upper mantle, Earth Planet. Sci. Lett. 234 (2005) 119–134.
[47] V.N. Zharkov, L.N. Dorofeeva, V.M. Dorofeev, V.M. Lyubimov, Distributions of dissipative function Q(l) in the Earth's shell, Izv. Akad. Nauk SSSR, Fiz. Zemli 12 (1974) 3–12.
[48] F.R. Boyd, High- and low-temperature garnet peridotite xenoliths and their possible relation to the lithosphere–asthenosphere boundary beneath southern Africa, in: P.H. Nixon (Ed.), Mantle Xenoliths, John Wiley, New York, 1987, pp. 403–412.
[49] N.V. Sobolev, Deep-seated Inclusions in Kimberlites and the Problem of the Composition of the Upper Mantle, Amer. Geophys. Union, Washington, DC, 1977, 279 p.
[50] L.V. Solovyeva, B.M. Vladimirov, L.V. Dneprovskaya, Kimberlites and Kimberlite-like Rocks. Upper Mantle Beneath Ancient Platforms, Nauka, Novosibirsk, 1994, 256 pp. (in Russian).
[51] W.F. McDonough, Constraints on the composition of the continental lithospheric mantle, Earth Planet. Sci. Lett. 101 (1990) 1–18.
[52] W.F. McDonough, R.L. Rudnik, Mineralogy and composition of the upper mantle, in: R.J. Hemley (Ed.), Ultrahigh-Pressure Mineralogy, Rev. Mineral., vol. 37, Mineral. Soc. Amer., Washington, DC, 1998, pp. 139–164.
[53] D. Francis, Cratonic mantle roots, remnants of a more chondritic Archean mantle? Lithos 71 (2004) 135–152.
[54] M. Grégoire, D.R. Bell, A.P. Le Roex, Garnet lherzolites from the Kaapvaal craton (South Africa): trace element evidence for a metasomatic history, J. Petrol. 44 (2003) 629–657.
[55] D.E. James, M.J. Fouch, J.C. VanDecar, S. van der Lee, Kaapvaal Seismic Group, Tectospheric structure beneath southern Africa, Geophys. Res. Lett. 28 (2001) 2485–2488.
[56] M. Zhao, C.A. Langston, A.A. Nyblade, T.J. Owens, Upper mantle velocity structure beneath southern Africa from modeling regional seismic data, J. Geophys. Res. 104B (1999) 4783–4794.
[57] R.E. Simon, C. Wright, E.M. Kgaswane, M.T.O. Kwadiba, The P wavespeed structure below and around the Kaapvaal craton to depths of 800 km, from traveltimes and waveforms of local and regional earthquakes and mining-induced tremors, Geophys. J. Int. 151 (2002) 132–145.
[58] M. Freybourger, J.B. Gaherty, T.H. Jordan, Kaapvaal Seismic Group, Structure of the Kaapvaal craton from surface waves, Geophys. Res. Lett. 28 (2001) 2489–2492.
[59] R.L. Saltzer, Upper mantle structure of the Kaapvaal craton from surface wave analysis — a second look, Geophys. Res. Lett. 29 (2002) (art. no. 1093).
[60] L. Vinnik, V. Farra, Subcratonic low-velocity layer and flood basalts, Geophys. Res. Lett. 29 (2002), doi:10.1029/2001GL014064.
[61] S.S. Gao, P.G. Silver, K.H. Liu, Kaapvaal Seismic Group, Mantle discontinuities beneath southern Africa, Geophys. Res. Lett. 29 (2002), doi:10.1029/2001GL013834.
[62] X. Qiu, K. Priestley, D. McKenzie, Average lithospheric structure of southern Africa, Geophys. J. Int. 127 (1996) 563–587.
[63] K. Priestley, Velocity structure of the continental upper mantle: evidence from southern Africa, Lithos 48 (1999) 45–56.
[64] R.E. Simon, C. Wright, M.T.O. Kwadiba, E.M. Kgaswane, Mantle structure and composition to 800-km depth beneath southern Africa and surrounding oceans from broadband body waves, Lithos 71 (2003) 353–367.
[65] J. Stankiewicz, S. Chevrot, R.D. van der Hilst, M.J. de Wit, Crustal thickness, discontinuity depth, and upper mantle structure beneath southern Africa: constraints from body wave conversions, Phys. Earth Planet. Inter. 130 (2002) 235–251.
[66] I.M. Artemieva, Lithospheric structure, composition, and thermal regime of the East European Craton: implications for the subsidence of the Russian Platform, Earth Planet. Sci. Lett. 213 (2003) 431–446.
[67] H. Thybo, E. Perchuć, The seismic 8° discontinuity and partial melting in continental mantle, Science 275 (1997) 1626–1629.
[68] L. Nielsen, H. Thybo, A.V. Egorkin, Implication of seismic scattering below the 8° discontinuity along PNE Profile Kraton, Tectonophysics 358 (2002) 135–150.
[69] O.L. Kuskov, V.A. Kronrod, Core sizes and internal structure of the Earth's and Jupiter's satellites, Icarus 151 (2001) 204–227.
[70] J. Kung, B. Li, T. Uchida, Y. Wang, D. Neuville, R.C. Liebermann, In situ measurements of sound velocities and densities across the orthopyroxene→high-pressure clinopyroxene transition in $MgSiO_3$ at high pressure, Phys. Earth Planet. Inter. 147 (2004) 27–44.
[71] A.B. Woodland, The orthorhombic to high-P monoclinic phase transition in Mg–Fe pyroxenes: can it produce a seismic discontinuity? Geophys. Res. Lett. 25 (1998) 1241–1244.
[72] F. Xu, J.E. Vidale, P.S. Earle, H.M. Benz, Mantle discontinuities under southern Africa from precursors to $P'P'_{df}$, Geophys. Res. Lett. 25 (1998) 571–574.
[73] O.L. Kuskov, V.A. Kronrod, L.L. Hood, Geochemical constraints on the seismic properties of the lunar mantle, Phys. Earth Planet. Inter. 134 (2002) 175–189.

[74] M.Q.W. Jones, Heat flow in the Witwatersrand basin and environs and its significance for the South African shield geotherm and lithosphere thickness, J. Geophys. Res. 93B (1988) 3243–3260.
[75] N. Sleep, Geodynamic implications of xenolith geotherms, Geochem. Geophys. Geosyst. 4 (9) (2003) 1079, doi:10.1029/2003GC000511.
[76] A. Deuss, J.H. Woodhouse, The nature of the Lehmann discontinuity from its seismological Clapeyron slopes, Earth Planet. Sci. Lett. 225 (2004) 295–304.
[77] W.F. McDonough, S.-s. Sun, The composition of the Earth, Chem. Geol. 120 (1995) 223–253.
[78] O.F. Gaul, W.L. Griffin, S.Y. O'Reilly, N.J. Pearson, Mapping olivine composition in the lithospheric mantle, Earth Planet. Sci. Lett. 182 (2000) 223–235.
[79] A. Dziewonski, D.L. Anderson, Preliminary reference Earth model, Phys. Earth Planet. Inter. 25 (1981) 297–356.
[80] B.L.N. Kennet, E.R. Engdahl, R. Buland, Constraints on seismic velocities in the Earth from traveltimes, Geophys. J. Int. 122 (1995) 108–124.
[81] M.G. Kopylova, J.K. Russell, Chemical stratification of cratonic lithosphere: constraints from the Northern Slave Craton, Canada, Earth Planet. Sci. Lett. 181 (2000) 71–87.
[82] C.-T.A. Lee, A. Lenardic, C.M. Cooper, F. Niu, A. Levander, The role of chemical boundary layers in regulating the thickness of continental and oceanic thermal boundary layers, Earth Planet. Sci. Lett. 230 (2005) 379–395.
[83] C.-T.A. Lee, R.L. Rudnick, Compositionally stratified cratonic lithosphere: petrology and geochemistry of peridotite xenoliths from the Labait volcano, Tanzania, in: J.J. Gurney, J.L. Gurney, M.D. Pascoe, S.H. Richardson (Eds.), Proc. 7th Intern. Kimberlite Conf., vol. 2, Cape Town, South Africa, 1999, pp. 503–521.
[84] M. Bizzaro, R.K. Stevenson, Major element composition of the lithospheric mantle under the North Atlantic Craton: evidence from peridotite xenoliths of the Sarfartoq area, southwestern Greenland, Contrib. Mineral. Petrol. 146 (2003) 223–240.
[85] J.C. Afonso, G. Ranalli, M. Fernàndez, Thermal expansivity and elastic properties of the lithospheric mantle: results from mineral physics of composites, Phys. Earth Planet. Inter. 149 (2005) 279–306.
[86] A.M. Doroshev, G.P. Brey, A.V. Girnis, A.I. Turkin, L.N. Kogarko, Pyrope–knorringite garnets in the Earth's mantle: experiments in the $MgO–Al_2O_3–SiO_2–Cr_2O_3$ system, Geol. Geophys. 38 (1997) 523–545.
[87] S. Klemme, The influence of Cr on the garnet–spinel transition in the Earth's mantle: experiments in the system $MgO–Cr_2O_3–SiO_2$ and thermodynamic modeling, Lithos 77 (2004) 639–646.
[88] S. Klemme, H.St.C. O'Neill, W. Schnelle, E. Gmelin, The heat capacity of $MgCr_2O_4$, $FeCr_2O_4$, and Cr_2O_3 at low temperatures and derived thermodynamic properties, Am. Mineral. 85 (2000) 1686–1693.
[89] A.M. Doroshev, V.M. Galkin, A.I. Turkin, A.A. Kalinin, Thermal expansion in the pyrope–grossular and pyrope–knorringite garnet series, Geochem. Int. 27 (1990) 144–147.
[90] T.J. Ahrens (Ed.), Mineral Physics and Crystallography: A Handbook of Physical Constants, Amer. Geophys. Union, Washington, DC, 1995.
[91] A.V. Girnis, G.P. Brey, Garnet–spinel–olivine–orthopyroxene equilibria in the $FeO–MgO–Al_2O_3–SiO_2–Cr_2O_3$ system: II. Thermodynamic analysis, Eur. J. Mineral. 11 (1999) 619–636.
[92] C. Long, N.I. Christensen, Seismic anisotropy of South African upper mantle xenoliths, Earth Planet. Sci. Lett. 179 (2000) 551–565.
[93] P.G. Silver, S.S. Gao, K.H. Liu, Kaapvaal Seismic Group, Mantle deformation beneath southern Africa, Geophys. Res. Lett. 28 (2000) 2493–2496.
[94] L.P. Vinnik, The mantle beneath the Kaapvaal Craton, South. Afr. Geophys. Rev. 2 (1998) 51–54.